A Microfabricated Solid Oxide Fuel Cell

by

Ankur Mehta

Submitted to the Department of Electrical Engineering and Computer Science and the Department of Physics
in partial fulfillment of the requirements for the degrees of
Master of Engineering in Electrical Engineering
and
Bachelor of Science in Physics
at the
MASSACHUSETTS INSTITUTE OF TECHNOLOGY
May 2004

© Ankur Mehta, MMIV. All rights reserved.

The author hereby grants to MIT permission to reproduce and distribute publicly paper and electronic copies of this thesis document in whole or in part.

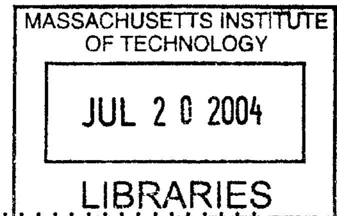

Author ....
Department of Electrical Engineering and Computer Science and the Department of Physics
May 20, 2004

Certified by ....
Martin A. Schmidt
Professor of Electrical Engineering
Thesis Supervisor

Certified by ....
Klavs F. Jensen
Professor of Chemical Engineering
Thesis Supervisor

Accepted by ....
Arthur C. Smith
Chairman, Department Committee on Graduate Students

BARKER

A Microfabricated Solid Oxide Fuel Cell

by

Ankur Mehta

Submitted to the Department of Electrical Engineering and Computer Science and
the Department of Physics
on May 20, 2004, in partial fulfillment of the
requirements for the degrees of
Master of Engineering in Electrical Engineering
and
Bachelor of Science in Physics

Abstract

With the ever-increasing ubiquity of mobile consumer electronic devices comes the rising demand for portable electric power. Current battery technology gives a very modest energy return per weight or volume. Hydrocarbons have a significantly higher energy density, and so fuel conversion systems only need to have several percent efficiency to match and surpass the specific energy of conventonal batteries. Thus, there is a strong market for successful portable fuel powered electric generators.

The goal of this thesis is to investigate the design of one such device, a two-chamber microfabricated solid oxide fuel cell (SOFC). This device produces electric current through the electrochemical oxidation of fuel through an ionic conductor. Oxide ions permeate across a ceramic electrolyte membrane to react with the fuel, driving electrons back around through the load. The focus of this work is to analyze the behavior of these membranes to prevent failure as the device is heated to its operating temperature near 800K.

Experiments and analysis of free-standing electrolyte membranes indicate that failure is unavoidable over the required temperature range, and so supported structures are investigated. The results of experiments with a perforated nitride supported membrane presented herein indicate the need for a more thorough understanding of the thin film stresses responsible for membrane failure, as well as careful support structures to accomodate these. Designs for future devices are presented to improve stability and move closer to a final complete portable power system.

Thesis Supervisor: Martin A. Schmidt
Title: Professor of Electrical Engineering

Thesis Supervisor: Klavs F. Jensen
Title: Professor of Chemical Engineering

Acknowledgments

This thesis is the culmination of a year of work that would not have been possible without the help and support of many people. First and foremost, I would like to thank my advisors, Profs. Klavs Jensen and Marty Schmidt. It has been a pleasure to work on this project, and their insight and assistance throughout has made this a great experience.

I have had much help from other grad students and postdocs during the year. My officemate, Ole Nielsen, has been an invaluable resource, and working alongside Dr. Ben Wilhite has helped me get through many of the difficulties I encountered. This project was greatly aided by the work of David Quinn, Josh Hertz, and Anja Bierble. I would also like to thank the other members of the MURI community, the Schmidt and Jensen Groups, and your mom for their insightful conversations and brainstorming sessions that drove this project forward.

This thesis would have never been finished had it not been for the relentless cries of "Stop slacking!" and "Thesis!" directed at me over the past month. The insistent poking and encouragement by my fellow Tetazooans, friends, and a little spirit forced me to tool through the weeks of warm sunny days, and kept me sane over the year.

Of course, I would like to thank my mom, dad, and sister for their continued love and support that has enabled me to be where I am today.

This research was made possible by grants from the Army Research Office Multi-disciplinary University Research Initiative (MURI).

Contents

1 Introduction **11**

2 Fuel Cells **13**

2.1 General Fuel Cell Operation 13

2.1.1 Power Conversion 13

2.1.2 Structure 13

2.1.3 Materials 14

2.2 Types of Fuel Cells 15

2.2.1 Proton Exchange Membrane Fuel Cell 15

2.2.2 Direct Methanol Fuel Cell 16

2.2.3 Solid Oxide Fuel Cell 16

2.3 Miniaturization 18

3 Design Considerations **21**

3.1 Heat Transfer 21

3.1.1 Conduction 21

3.1.2 Convection 22

3.1.3 Radiation 23

3.2 Thin Film Stress 24

3.2.1 Thermal stress 24

3.2.2 Intrinsic stress 25

3.2.3 Composite films 27

3.3 Membrane Mechanics 27

3.3.1 Buckling 27

3.3.2 Bending 28

3.3.3 Fracture 28

3.3.4 Design Space 29

4 Test Structures and Devices 31
4.1 Research Paths 31
4.2 Etching and Chemical Compatibility 31
4.3 Free Standing Test Membrane Structure 33
4.4 Perforated Support Membrane Structure 36
4.5 Composite Film Test Membrane Structure 39

5 Testing Results 41
5.1 Electrolyte Selection 41
5.2 Supported Membranes 42
5.3 Stress and Film Characterization 48
5.3.1 YSZ Electrolyte Films 48
5.3.2 Pt-YSZ Electrode Films 49

6 Proposed Designs 51
6.1 Membrane Robustness 51
6.1.1 Honeycomb Supported Membranes 51
6.1.2 Corrugated Membranes 52
6.2 Integrated Portable Power System 54

7 Conclusion 59

A Test Membrane Array Process Flow 61

B Test Membrane Array Masks 65

C Holy Membrane Process Flow 69

D Holy Membrane Masks 75

List of Figures

2-1 Schematic of a general fuel cell structure 14
2-2 Schematic of a single-sided fuel cell structure 15
2-3 Minimum operating temperature for given electrolyte thickness 18

3-1 Origin of compressive stress in CVD thin films 26
3-2 Origin of tensile stress in CVD thin films 26
3-3 Design space for successful thin film membranes 30

4-1 Diagrammed process flow for test membrane arrays. 34
4-2 Diagrammed revised process flow for test membrane arrays. 35
4-3 Diagrammed process flow for the "holy" membrane device. 37

5-1 Buckled and fractured YSZ test membranes 42
5-2 A holy membrane buckled after YSZ deposition 44
5-3 A closer look at buckling on a supported YSZ membrane 44
5-4 A YSZ holy membrane after anneal showing regions of film delamination 45
5-5 A closeup on delaminated regions showing buckling 46
5-6 Remnants of an e-beam deposited YSZ supported membrane 47
5-7 A cracked and peeling Pt-YSZ/YSZ/Pt-YSZ film stack 47

6-1 A sample process flow for a honeycomb supported membrane device. 53
6-2 A sample process flow for a corrugated membrane device. 55
6-3 Potential integrated power system device design 56

B-1 Nitride etch mask for square variable area test membranes 65

B-2 Nitride etch mask for variable aspect ratio test membranes 66
B-3 Die-level nitride etch mask for variable aspect ratio test membranes . 67

D-1 Die-level masks for holy membrane process 75
D-2 Close-up view of membrane masks 76
D-3 Flowchannel etch mask in holy membrane process 77
D-4 Die-level flowchannel etch mask 77
D-5 Perforation etch mask in holy membrane process 78
D-6 Die-level perforation etch mask 78
D-7 $4\mu m$ perforations in etch mask 79
D-8 Metalization liftoff mask in holy membrane process 79
D-9 Die-level metalization liftoff mask 80
D-10 Temperature sensing wire loop inside heating wire loop on membrane 80
D-11 Insulation liftoff mask in holy membrane process 81
D-12 Die-level insulation liftoff mask 81

Chapter 1

Introduction

With the progress of microtechnology came the proliferation of portable electronic devices. Cell phones, laptops, and GPS receivers are but of a few of the many devices which have almost become indispensable. These all require electrical power to operate. Currently, this is supplied by various types of primary (single use) and secondary (rechargeable) batteries. However, in terms of energy densities, batteries store almost an order of magnitude less energy per weight or volume than hydrocarbon fuels. One method of harnessing this hydrocarbon energy is through the use of fuel cells, which electrochemically oxidize the fuel to generate power.

There are several types of fuel cells, of which most have been successfully operated in macroscale dimensions. Solid oxide fuel cells (SOFC's), which function by transporting oxide ions through an electrically insulating electrolyte, currently show high efficiency and also allow the direct use of a hydrocarbon fuel rather than pure hydrogen. However, to effectively use fuel cells to provide portable power, the systems must be miniaturized to scale with the microelectronic devices. As such, this research will be towards the realization of a microfabricated SOFC.

Miniaturization carries with it several challenges. One issue that must be dealt with is heat transfer and containment. For a solid oxide fuel cell to function effectively, the electrolyte must be kept at elevated temperatures, around 800 K. On a microscale, the surface area to volume ratio is very high, and so heat is dissipated very quickly to the surrounding gasses. Furthermore, the device is built on a silicon substrate, which

acts as a significant thermal mass absorbing a large amount heat for even a small temperature difference. A structure must be designed to minimize the power input needed to keep the membrane at the appropriate temperature.

With the electrolyte, most often in the form of a membrane separating the fuel and oxygen, needing to be at a high temperature, mechanical stability concerns become relevant. At high temperatures, changes in the crystal grain structure of the electrolyte material give rise to stresses in the film. With larger membrane dimensions, this can cause fractures. A mismatch in the coefficients of thermal expansion between the membrane and the substrate also add stresses. Changes in geometry and fabrication steps can have a strong impact on the mechanical robustness of a design.

The complete SOFC design additionally consists of thin film electrodes on either side of the electrolyte. These serve both as a catalyst for the appropriate half-reaction, as well as a current collector conducting the electrons to and from terminals. These need to provide enough triple-phase sites, where the gas meets the ionic and electronic conductors, for the reaction to take place, while having sufficiently low resistance to cause minimal power loss. The materials for these electrodes are often more complex than the electrolyte and so introduce their own chemical and mechanical limitations.

These considerations, when all taken into account, create a tight design space in which to work. The work presented in this thesis examines these conditions and their impact on a successful design of a microfabricated SOFC. The insight gained through experiments conducted over the year is presented, and the critical problems remaining to be solved in order to achieve such a portable power device are identified. Designs for future investigation of these challenges are also proposed.

Chapter 2

Fuel Cells

2.1 General Fuel Cell Operation

2.1.1 Power Conversion

A fuel cell is a device that electrochemically oxidizes hydrocarbons in order to generate an electric current. The crux of the device is an ionic conductor that separates the fuel from oxygen. This electrolyte is an electrical insulator but transports ions between the oxygen and the fuel. The various types of fuel cells differ in the operating properties of this electrolyte, which usually transports either hydrogen or oxygen ions.

Electrochemical half-reactions occur at the interface of the electrolyte with catalytic electrodes on each side. Electrons are given up at the anode and recombine at the cathode. The circuit is then completed across a load. A schematic of fuel cell operation is shown in figure 2-1.

2.1.2 Structure

Fuel cells must be designed such that fuel and oxygen do not combine directly with each other but are forced to react through the electrolyte. The easiest way to achieve this is by creating a two chamber fuel cell, as in the schematic in figure 2-1. The fuel and oxygen are kept separate by the electrolyte and can only react via ions sent through this membrane. The actual shape of these chambers is arbitrary; existing

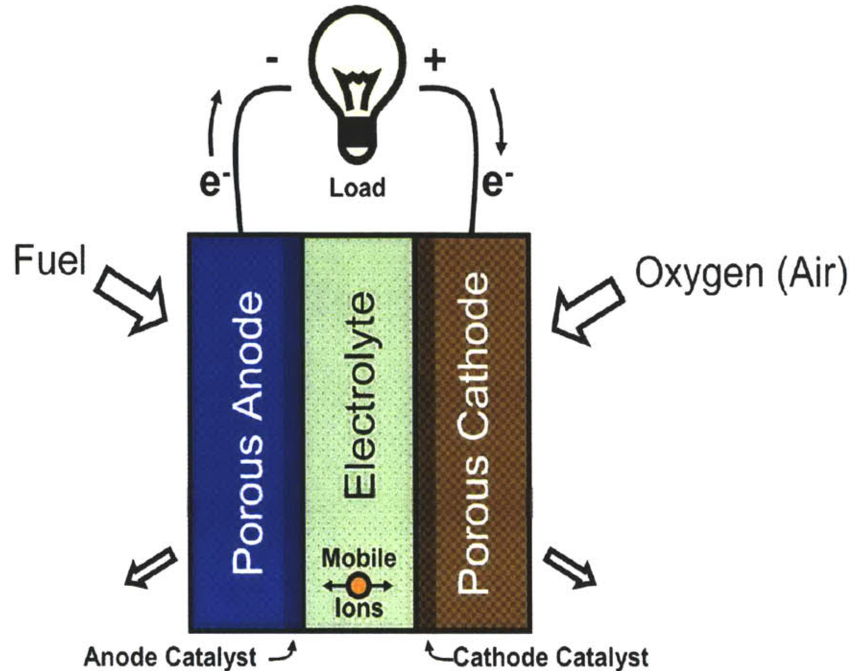

Figure 2-1: Schematic of a general fuel cell structure. Depending on the type of fuel cell, the electrolyte can transport either hydrogen or oxygen ions.

designs include tubes, plate stacks, and channels.

It is possible to make a single chamber fuel cell, where a mixture of fuel and air is sent over the electrolyte. The two specially selected electrodes would need to strongly catalytically favor their respective half-reactions to prevent combustion. The ions would then flow in the plane of the electrolyte between the electrodes. This configuration is seen in figure 2-2.

2.1.3 Materials

The electrolyte properties are critical to the performance of the fuel cell. It must have a high ionic conductivity to avoid transport losses but must also have a high electrical resistance to force the generated current through the load. Furthermore, it must be impermeable to the fuel and oxygen and itself not react reversibly with the reactants, products, or associated species.

The electrodes must satisfy similar chemical compatibility requirements and have a high electrical conductivity to minimize ohmic losses. They should also catalyze

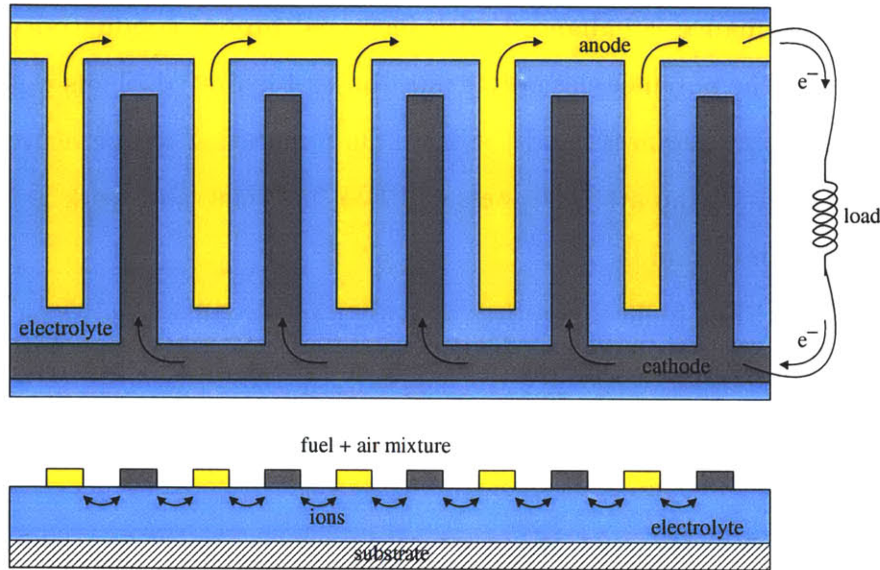

Figure 2-2: Schematic of a single-sided fuel cell structure

their respective half-reactions. Since the electrodes provide electron transport while the electrolyte provides the ionic transport, each half-reaction can only occur at the triple-phase boundaries where the gas and these two materials are all in contact. Thus, the electrodes must either be porous to allow the gases to flow to the electrolyte, or else consist of a composite including both electronic and ionic conductors.

2.2 Types of Fuel Cells

2.2.1 Proton Exchange Membrane Fuel Cell

The electrolyte in a proton exchange membrane (PEM) fuel cell (also known as polymer electrolyte membrane fuel cells) is typically a hydrated polymer that is conductive to hydrogen ions, or protons. It uses pure hydrogen as the fuel and ionizes it at the anode. The protons are conducted through the electrolyte, while the electrons are sent through the load. These combine with oxygen at the cathode to produce water.

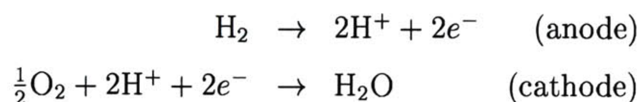

$$\begin{aligned} \mathrm{H_2} &\rightarrow 2\mathrm{H}^+ + 2e^- && \text{(anode)} \\ \tfrac{1}{2}\mathrm{O_2} + 2\mathrm{H}^+ + 2e^- &\rightarrow \mathrm{H_2O} && \text{(cathode)} \end{aligned}$$

Fuel cell performance is enhanced with increased proton conductivity at higher temperatures, but the polymer electrolyte must be kept hydrated. Thus water restoration systems are often required, and the maximum operating temperature is limited to 80°C. These reduce the attractiveness of PEM fuel cells, and work is being done to overcome this limitation [1, 16].

Additionally, a PEM fuel cell requires a highly pure stream of hydrogen fuel. Thus a complete system requires either direct hydrogen storage or a hydrocarbon reformer with a hydrogen purifier to provide the fuel.

2.2.2 Direct Methanol Fuel Cell

A direct methanol fuel cell (DMFC) operates very similarly to the PEM fuel cell above, with methanol reacting with water at the anode to produce the hydrogen ions and carbon dioxide.

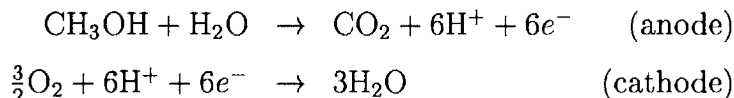

$$\begin{aligned} CH_3OH + H_2O &\rightarrow CO_2 + 6H^+ + 6e^- \qquad \text{(anode)} \\ \tfrac{3}{2}O_2 + 6H^+ + 6e^- &\rightarrow 3H_2O \qquad \text{(cathode)} \end{aligned}$$

The same structure (with different catalysts) can often be used as either a PEM or DMFC, with the DMFC providing the added benefits of eliminating the need for pure hydrogen [21].

However, methanol must be sufficiently diluted with water in order for the reaction to proceed. Storing the methanol pre-diluted eliminates the benefits of using a fuel other than hydrogen. Alternatives require sensors and feedback to maintain appropriate methanol concentrations but still lose efficiency over hydrogen based systems [20].

2.2.3 Solid Oxide Fuel Cell

In a solid oxide fuel cell (SOFC), the electrolyte conducts oxygen ions generated at the cathode to the anode. There, it combines with the fuel, generally hydrogen, to produce free electrons. These are sent through the load to the cathode where they

combine with oxygen to produce oxygen ions and complete the circuit.

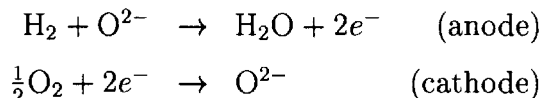

$$
\begin{aligned}
H_2 + O^{2-} &\rightarrow H_2O + 2e^- && \text{(anode)} \\
\tfrac{1}{2}O_2 + 2e^- &\rightarrow O^{2-} && \text{(cathode)}
\end{aligned}
$$

There has been much research into oxide conductors for this electrolyte, which tend to be complex rare earth oxides. The current popular choice for electrolyte material is yttria-stabilized zirconia (YSZ), although other ceramics like gadolinium doped ceria (GDC) are being investigated. These ceramics provide the requisite oxide conductivity with good electrical insulation [9].

In order to achieve high oxide conductivities, the electrolyte must be kept at a very high temperature. A minimum operating temperature, depending on film thickness, in the hundreds of degrees Celsius is necessary to keep the losses through the electrolyte below some threshold. This is shown in figure 2-3, taken from [5]. It is seen that YSZ requires thinner films for a given operating temperature to achieve losses comparable to GDC.

With the high electrolyte temperatures required for operation, it becomes possible for an SOFC to use fuels other than hydrogen. The anode often provides catalytic support for hydrocarbon reforming, thus producing hydrogen which in turn reacts with the oxygen ions. It is also possible for the oxygen ions to combine directly with the hydrocarbons themselves [13].

There are many materials under consideration for use as SOFC electrodes. Platinum is an excellent conductor and catalyst, however it is expensive and must be made porous to provide sufficiently many three-phase boundaries. Alternately, it can be mixed with an ionic conductor to make a ceramic-metal composite (cermet). Nickel-YSZ is another such cermet that is currently favored. Perovskites like lanthanum strontium manganate (LSM) are part of an alternate class of electrodes. These are mixed ionic and electric conductors that permit transport of both types of charged reagents.

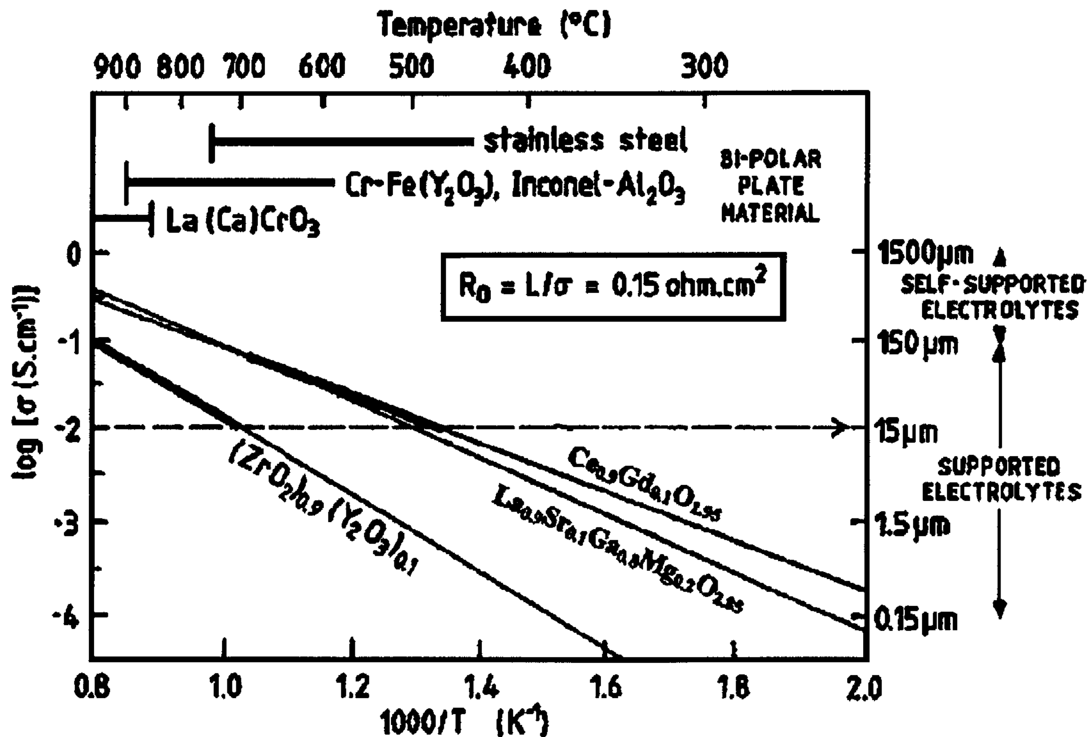

Figure 2-3: Minimum operating temperature for given electrolyte thickness[5]

2.3 Miniaturization

The high energy density of fuels makes it an attractive potential source of portable power. Demand for electrical power in consumer appliances is ever-growing, and there is always a call for smaller, cheaper, and more efficient sources. Currently batteries service most of the portable electric needs but they store orders of magnitude less energy per weight than hydrocarbon fuels. A power conversion device of only several percent efficiency would then outperform batteries [20].

Thus, there has been much work into miniaturizing fuel conversion systems. These range from simple devices that combust the fuels for heat to complicated turbine driven generators. A combustive heat source can be coupled to a heat sink through a thermopile to form a thermoelectric generator, as devised in [20]. It can be used to radiate photons, which then produce electric power at a photocell in a thermophotovoltaic generator as in [14]. Micromechanical gas turbine engines have undergone much research also, for example in [7].

The relative simplicity of fuel cell systems then makes it an excellent candidate for miniaturization to provide portable power. This can be accomplished using conventional manufacturing processes and fuel cell techniques but on a smaller scale, e.g. in [4, 6, 18, 25]. However, it is also possible to use the microelectromechanical system (MEMS) paradigm to microfabricate devices using batch IC processing techniques.

MEMS fuel cells carry several advantages over miniaturized conventional fuel cells. Primarily, smaller dimensions can be achieved through microfabrication, allowing for thinner electrolyte layers. This correspondingly reduces its ionic resistance and allows for lower operating temperatures. Furthermore, conceivable MEMS designs have potential for more ideal thermal strategies, in terms of inhibiting heat losses to the environment while providing for efficient heat transfer when required [3].

Without any moving parts, microfabricated fuel cells become an attractive option for the realization of a microchemical power production device. In fact, there has been much prior research into designing such systems. Much of the work has focused on PEM fuel cells, mostly due to their low operating temperatures [11, 17]. These require a hydrogen fuel source, either directly or from the output of a complex fuel reforming/purifying system. Either adds to the weight and volume of the final system, negating much of the benefit over batteries.

Direct methanol fuel cells have also been attempted to overcome the requirement of hydrogen fuel. However, these have problems with methanol cross-over at the required concentrations for operation [6, 18]. Furthermore, both PEM and DMFC's require hydrated polymer membranes, with complicated water recovery or delivery systems to maintain the electrolyte.

Solid oxide fuel cells, on the other hand, potentially allow for the direct utilization of hydrocarbon fuels, with well studied electrode and electrolyte materials. The primary challenge in microfabricating SOFC's, then, is to handle the complexities arising from their thermal requirements. The potential win from a successful micro SOFC is thus worth the design effort, and there have been other attempts to create such a device [11].

Chapter 3

Design Considerations

The goal of this work was to create a microfabricated fuel cell. A single-sided SOFC design calls for a highly explosive fuel/air mixture flowing over a catalyst at high temperatures. Thus it was ruled out, leaving the two chamber design as the primary target. It became quickly apparent that the major focal point for development work needed to be on the membrane separating the fuel and oxygen flows.

3.1 Heat Transfer

Efficient operation of a solid oxide fuel cell requires that the electrolyte be heated to high temperatures. Maintaining that temperature against room temperature gas flows and in an ambient environment requires continuous power input. For the fuel cell to be a viable portable power device, heat losses from the membrane must therefore be minimized. The system should be designed to reduce conductive, convective, and radiative losses.

3.1.1 Conduction

Conduction is the heat transfer from hot to cold regions through a generally solid or liquid thermally conductive material. A temperature gradient gives rise to a heat flux

Φ through the cross-sectional area of the conductor given by

$$\Phi = -k\nabla T$$

which for a one dimensional heat flow between two temperature reservoirs over length L reduces to

$$\Phi = -\frac{k}{L}(T_H - T_C).$$

If the membrane is supported by a room temperature substrate, a gradient will develop over the surface. Heat will flow out from the heated reaction zone to the colder edges. Analysis of a model membrane under uniform heating suggests that even a slight temperature difference to the substrate incurs significant conductive losses, with a power loss greater than can be expected for the device to produce [23]. This suggests that despite using a poorly conductive thin film membrane for thermal isolation, membrane heating alone is not a viable solution.

This then requires the supports as well as the membrane to be kept at an elevated temperature. Since the final device must be usable in a room temperature environment, conduction paths between the reaction zone and the packaging must be eliminated. A microreactor has been designed in [2], which provides strong insulation through the use of a reaction zone suspended by thin-walled silicon nitride tubes. The small cross sectional area of the tubes coupled with the poor conductivity of nitride slash conductive losses.

3.1.2 Convection

Convection is the transfer of heat from a surface through fluid motion. It actually follows a complicated dependence on surface type, fluid properties, and physical geometries. However, the rate of heat transfer is proportional to surface area and temperature difference between the surface and bulk fluid, with the constant of proportionality empirically determined based on the other properties.

The membrane in the fuel cell will be surrounded on both sides by gas flows, and

so convective losses cannot be eliminated. Forced convection will cause the exhaust streams to carry away some of the heat from the membrane. However, less heat gets transferred to the gasses the warmer they are, and so convective losses can be minimized by heating the gasses before contact with the membrane.

A heat recovery system has been designed in a gas flow microscale chemical reactor in [2]. In that, highly thermally conductive silicon busbars transfer heat from the warm exhaust to the incoming room temperature gas flows. This system was shown to reduce convective heat losses by up to 50% at reasonable flow rates.

Convection can also cause heat loss to the environment from any other heated components of the final system. In a system where the device substrate is also heated, energy can be dissipated to the surrounding atmosphere. This problem can be eliminated by packaging the device in a vacuum; research into this scheme is ongoing.

3.1.3 Radiation

Finally, every surface also loses energy due to radiation based on its temperature. This is characterized by the Stefan-Boltzmann law for radiative heat flux over the area of the surface Φ:

$$\Phi = \epsilon \sigma T^4$$

where ϵ is the emissivity of the surface and $\sigma = 5.67 \times 10^{-8} JK^{-4}m^{-2}s^{-1}$ is the Stefan-Boltzmann constant.

Radiative heat losses are generally of a smaller magnitude than the other two methods, nonetheless, it still dissipates energy. Appropriate design can minimize conductive and convective losses, then bringing radiation to the forefront. Reducing the emissivity of the surfaces of the heated regions, e.g. by coating them with low emissivity materials, reduces the radiated heat flux. Also, by surrounding the heated sections in reflective packaging, the radiated energy can be directed back at the device to restore the heat.

An alternative is convert the radiated energy into electric power. Photovoltaic cells are designed do just that, and there has been much research into such ther-

mophotovoltaic power production devices. A design has been proposed in [14] to use a heated microreactor to radiate onto a photocell to deliver portable power.

3.2 Thin Film Stress

The fuel cell stack in an SOFC device consists of thin films of materials formed by chemical vapor deposition (CVD) anchored to a silicon substrate. This substrate is etched away in regions to release the membranes. In addition to geometry, the behavior of these membranes is strongly dependent on the stress in the thin films.

3.2.1 Thermal stress

Thermal stresses arise from thermal expansion behavior. As the temperature of a material increases, the molecules experience a greater magnitude of thermal motion, increasing the space occupied by the atoms. Most materials behave linearly, with a change in linear dimension directly proportional to the temperature change

$$\frac{\Delta L}{L} \propto \frac{\Delta T}{T}.$$

The proportionality constant is known as the coefficient of thermal expansion (CTE).

If a deposited thin film has a CTE different than that of the substrate material, changes in temperature would result in a different amount of growth in the two. With good adhesion of the film to the substrate, however, the film is constrained to expand in the same manner as the much thicker substrate. This induced strain gives rise to the thermal stress σ_{th} over a temperature change ΔT

$$\sigma_{th} = \frac{-E}{1-\nu}(\alpha - \alpha_s)\Delta T,$$

where E and ν are the Young's modulus and Poisson's ratio respectively of the thin film material, and α and α_s are the CTE's of the thin film and substrate [28].

If the thermal expansion coefficient of a thin film is greater than that of its sub-

strate, heating would drive the stress more compressive while cooling would drive it more tensile. The opposite is true for films of lower CTE than the substrate. This calculation gives the additional thermal stress in a film as its temperature changes from a base case. If the film is unstressed at room temperature, than raising the temperature would increase the magnitude of the stress in the film.

However, it is also possible to have a residual thermal stress in the film at room temperature. Materials are often deposited at elevated temperatures. Near a significant fraction of the material's melting point, the crystal grain structure can modify itself on the structure to accommodate strain, thus creating an unstressed configuration at higher temperatures. Then, the magnitude of the stress would increase as it is cooled to room temperature, and decrease as the temperature is raised.

3.2.2 Intrinsic stress

As deposited, thin films can also carry a residual intrinsic stress in addition to thermal stress, due to deposition processes and conditions. This can be tensile or compressive in nature.

Compressive stress tends to arise from forward sputtering effects, also known as atomic peening. Atoms arriving at the surface are driven into the existing crystal in locations other than prescribed by the lattice points. The energy of impact as the material is deposited can embed the arriving atom at these unfavorable locations, or incoming atoms can knock already deposited atoms loose, which then travel deeper into the film. The energy of this close packing of atoms is manifest in the compressive stress. This is depicted figure 3-1.

Tensile stress in deposited thin films occur due to boundaries in the crystal grain structure. Surface atoms have higher energy than internal atoms. Thus, surface tension effects tend to pull isolated grain boundaries into spherical surfaces. However, as grains come in contact with their neighbors, the surfaces would rather join to minimize surface energy. This tends to "zip" up the boundaries, pulling the grains closer together, and resulting in tension in the film. This is demonstrated in figure 3-2 taken from [15].

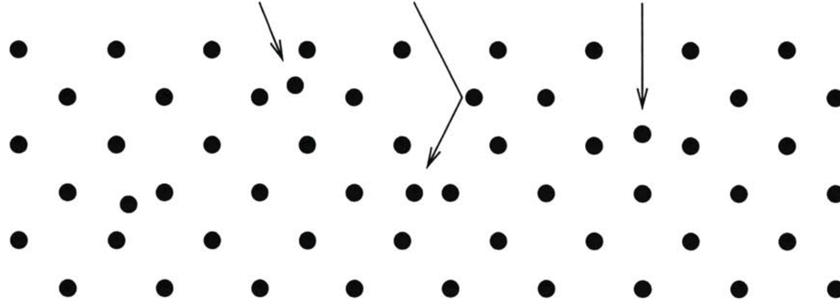

Figure 3-1: Compressive stress in CVD thin films is caused by forward sputtering. Incident atoms are driven into crystal structure, packing the atoms more tightly. [15]

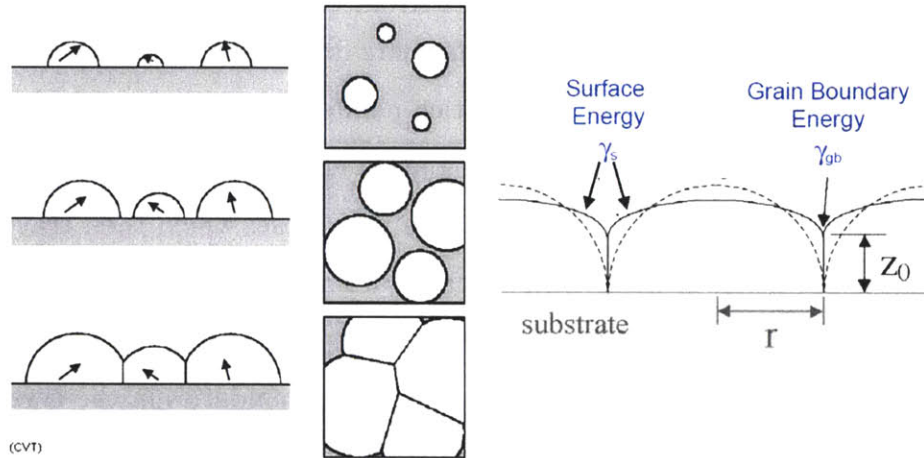

Figure 3-2: Tensile stress in CVD thin films is caused by the balancing of the grain surface energy with the boundary energy. [15]

These two effects provide competing stresses, and thus intrinsic stress in deposited films can vary from strongly tensile to strongly compressive. Processing conditions can affect the balance between these, and minor adjustments can drive a deposited film from one side to the other.

3.2.3 Composite films

Stress considerations grow in complexity as film stacks are used. Individual film stress components can be added based on thickness to give the overall membrane stress. However, multi-layer stacks with different film stresses give rise to internal moments along the membrane. In particular, a tensile film deposited on a compressive film may have no net stress, but the internal bending moment may still cause it to be deflected at rest.

Additional complications arise from the interface between the films. Differential stresses between layers can overcome the chemical adhesion, and result in delamination. This behavior is very difficult to model, and is best treated experimentally.

3.3 Membrane Mechanics

3.3.1 Buckling

An unstressed membrane is initially in stable equilibrium in a flat configuration. As compressive stress increases in the membrane, possibly by raising the temperature, the membrane remains flat until a point. At this critical stress, the equilibrium bifurcates, giving rise to a stable deformed equilibrium state, and the flat equilibrium state becomes unstable. The membrane will then spontaneously deflect to a stable equilibrium configuration. This phenomenon is called buckling.

A circular membrane on a stiff substrate can be modeled as a plate with fixed (clamped) boundary conditions. Analysis of this problem gives a critical buckling

stress σ_{cr} for a plate or radius b and thickness h [24, 26]

$$\sigma_{cr} = -1.22\frac{E}{1-\nu^2}\left(\frac{h}{b}\right)^2.$$

It is immediately seen that thicker, smaller membranes are more robust against buckling. However, this is contrary to fuel cell performance, where thinner films are more efficient, and the reaction occurs across the surface area. Thus there is a tradeoff that must be satisfied by appropriate design.

3.3.2 Bending

A membrane below the buckling limit may still adopt a deformed configuration. A multilayered composite film structure with layers of different stress will have a bending moment along the extent of the membrane. This moment will deflect the membrane such that the stable equilibrium is in a deformed rather than flat configuration. The curve will tend to be more gentle than those formed by buckling, but occur at lower stresses. In fact, a nominally unstressed bilayer may experience bending regardless of additional thermal stresses.

3.3.3 Fracture

Similar to the critical buckling stress for compressive membranes, there is a stress above which a film in tension fails. This is primarily caused by the propagation of cracks, which form near the fracture strength of the material, σ_f. This quantity carries a complex dependence on a variety of factors, and is most often simply experimentally determined or fit to numerical models.

It is important to note that this stress limit a local one, and fractures can develop anywhere there is significant stress concentration. In particular, a significantly compressive film may buckle, and develop ridges with a sharp curvature. The outer face of this curve could undergo sufficient tensile strain to induce failure, and cause the membrane to rupture. It is also plausible that this could occur in a simply bent film.

3.3.4 Design Space

The above constraints on membrane failure due to buckling or fracture can be combined with the analysis for induced thermal stresses to produce a design map for membrane stability. The basic model gives the total stress in the film is the sum of the intrinsic and thermal stresses, and it is this stress that must be between the bounds of failure. Since the device must be stable at room temperature, the intrinsic stress must be between σ_{cr} and σ_f. Then, assuming a material of greater CTE than the substrate, a maximum temperature change is allowable such that the total stress remains less than σ_{cr}. This is diagrammed in figure 3-3 from [23].

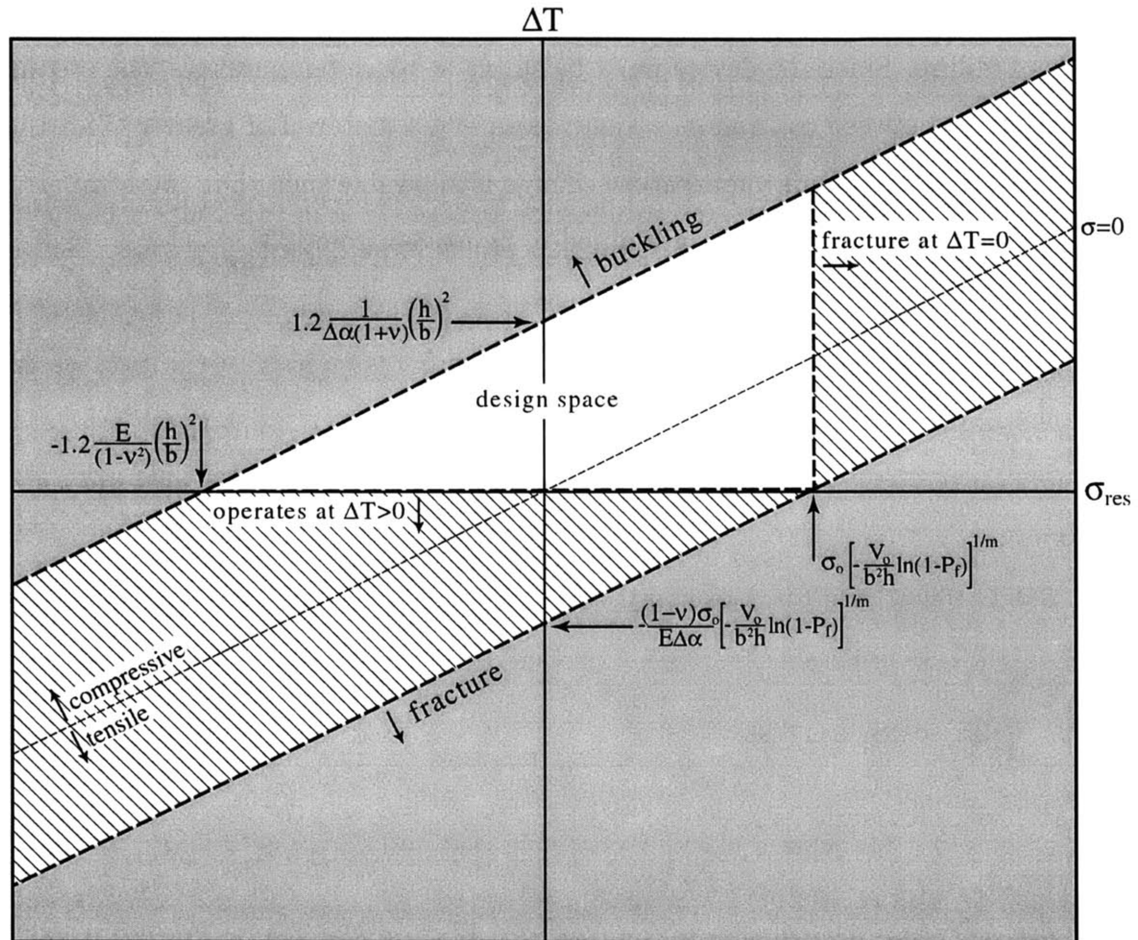

Figure 3-3: The membrane thin film carries an intrinsic residual stress, compressive to the left. With an imposed temperature change, the total film stress must remain between the buckling and fracture limits in order to survive. With the requirement that the membrane be stable at room temperature ($\Delta T = 0$), the white triangle contains geometries resistant to failure. [23]

Chapter 4

Test Structures and Devices

4.1 Research Paths

The successful realization of a membrane based dual-chamber SOFC requires the careful understanding of many different disciplines. The basic principle of the fuel cell operation is fundamentally chemical in nature, and implementation requires specific materials. A stable membrane structure must be designed around these materials that can also satisfy the thermal and fluidic requirements of SOFC operation. Finally, this device must be realizable in available microfabrication processes.

Indeed, this project is part of a multidisciplinary team, with various research groups working in parallel on different aspects of the problem. Research was conducted elsewhere on chemical composition and deposition techniques of the fuel cell materials, structural modeling of the membrane, and complete system modeling. The work done for this thesis focused on the design and fabrication aspects of creating a SOFC device, and in particular the membrane support for the fuel cell stack.

4.2 Etching and Chemical Compatibility

A key process step in many MEMS devices is the selective removal of material through chemical etches. The structures fabricated in this work are no different.

The membranes are defined through the removal of silicon with a wet potassium

hydroxide (KOH) etch. KOH has a strong etch selectivity to the {100} and {110} planes over the {111} plane, and so masked features on a (100) Si wafer etch into inverted pyramids with rectangular bases and {111} sidewalls. These walls are sloped at 54.7°, and the released membranes will then be smaller than the mask feature size. The relationship of the size of the membrane $l_{membrane}$ created by a given mask dimension l_{mask} in a (100) wafer of thickness t is:

$$l_{membrane} = l_{mask} - \frac{2t}{\tan(54.7^\circ)}.$$

KOH etches silicon dioxide a thousand times slower than the {100} silicon plane and does not etch silicon nitride at all, so both make good KOH hardmasks. SiO_2 can be etched with hydrofluoric acid (HF) or a buffered oxide etch (BOE) solution of HF and ammonium fluoride. Nitride, both stoichiometric and low-stress VTR, is dry etched with in fluorine (SF_6) plasma or wet etched in hot phosphoric acid.

It becomes important to ensure chemical compatibility with materials that may come in contact with these etchants during processing. In particular, the fuel cell materials must be able to withstand the membrane processing, or be suitably protected if they cannot. Earlier tests determined that YSZ was indeed resistant to KOH. An SF_6 plasma etch was also shown to be highly selective to silicon and nitride over YSZ and GDC [3].

To determine the selectivity of BOE, samples were prepared with YSZ and GDC deposited on half a piece of silicon. Profilometry measurements determined the thickness of the electrolyte layer. The samples were dipped in a BOE solution for a range of times, then washed and remeasured. YSZ showed no thickness loss measurable over the surface roughness, whereas GDC was completely etched away over a two minute dip. Literature verifies the extremely slow etch rate of YSZ in HF [27].

4.3 Free Standing Test Membrane Structure

The key impetus for developing a microfabricated SOFC is to allow for thinner electrolyte films. However, regardless of the relative dimensions, the electrolyte is always a dense film. The electrode layers are often desired to be porous, to allow a greater number of three phase reaction sites. Thus, the initial design goal was to create an electrolyte-supported fuel cell film stack.

As such, previous research on the structural stability of the required membranes began with an analysis of free standing YSZ or GDC electrolyte films [3]. Square membranes of varying side length are formed on a silicon die. Since the thin films need to be deposited on a continuous surface, the membranes are released after deposition by removing the silicon substrate with a wet KOH etch.

The process flow is diagrammed in figure 4-1. Initially, a low stress (VTR) nitride layer is deposited over a 4" (100) silicon wafer in which to define a hard mask. This mask, shown in figure B-1, is patterned in standard positive resist spun over the back side of the wafer. Following development of the resist, which removes exposed resist (in the clear regions of the mask), the plasmaquest reactive ion etcher is used to etch the defined features clear of the nitride. The wafer is then ready to have the electrolyte layer deposited.

Following the deposition, the wafer is etched in KOH to define the membranes. The exposed circular regions etch into inverted square pyramids with $\{111\}$ faces. Since the mask is circular, small deviances in alignment of the mask with respect to the crystal axes still result in squares of the same dimension.

The final step is to release the free standing membranes to leave only the electrolyte material. Since the nitride is to be removed in a reactive ion etch, it needs to be timed to avoid affecting the electrolyte film. This is calibrated by masking off some membranes during the electrolyte deposition and then examining these after the timed etch. The correct etch would completely clear these membranes of material.

A slightly modified process, based on the "holy" membrane process explained in the following section, was later adopted instead. This is listed in appendix A and

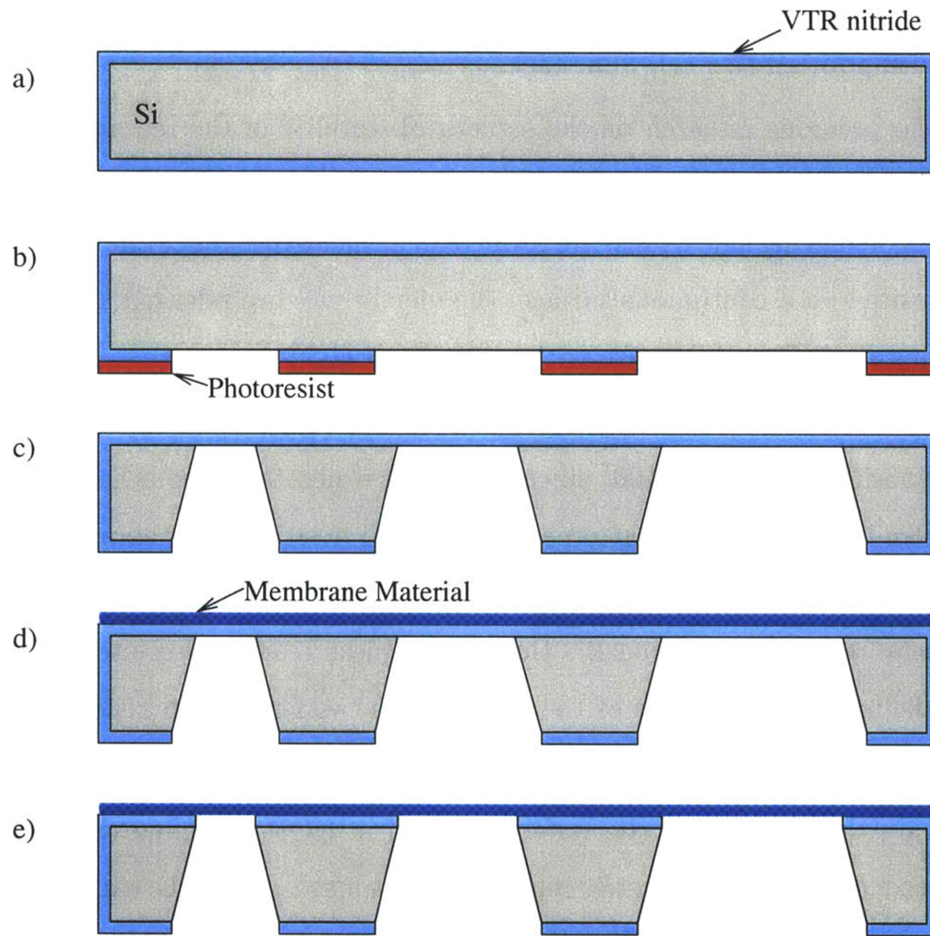

Figure 4-1: Stages in the process to create an array of test membranes: (a) VTR (low-stress) nitride coated (100) wafer (b) Membrane cavity hardmasked in nitride by etching through photoresist mask (c) Membranes formed in KOH (d) Fuel cell materials deposited on top of membrane. (e) Membranes released with nitride etch.

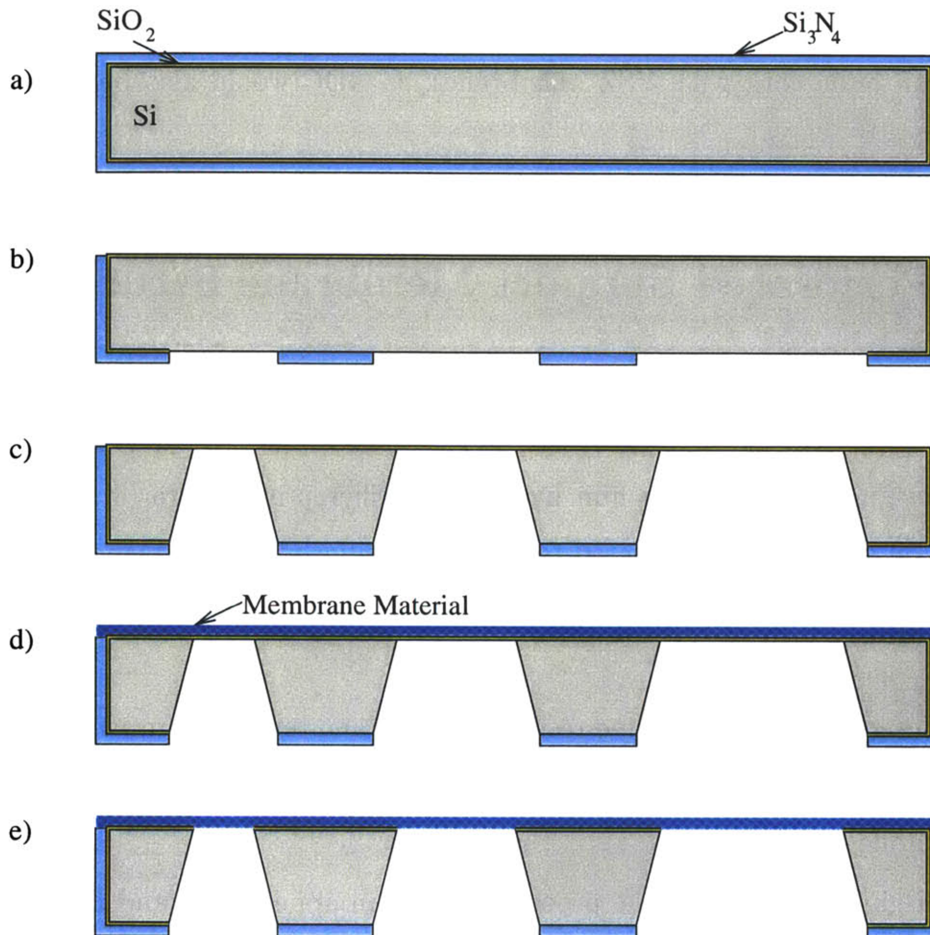

Figure 4-2: Stages in the revised process to create an array of test membranes: (a) Nitride and oxide coated (100) wafer (b) Membrane cavity hardmasked in nitride and oxide and frontside nitride stripped (c) Membranes formed in KOH (d) Fuel cell materials deposited on top of membrane. (e) Membranes released in BOE.

diagrammed in figure 4-2. It eliminates the need for a precise timed etch, as well as the dependence on the unreliable VTR nitride tube, which is often down for maintanance. This process was used both with the square membranes, as well as a set of membranes of varying aspect ratios, as shown in figure B-2.

A thermal oxide is first grown on the bare silicon wafers, following which a stoichiometric nitride layer is deposited. The thicknesses are selected to balance the residual stresses in these films. The membrane geometries are hardmasked in both of these layers, and the nitride is completely stripped off of the front. The rest of the process proceeds as above, but instead of a timed nitride etch to release the mem-

brane at the end, a BOE wet etch is used to remove the oxide layer completely. This process can only work with YSZ membranes, as GDC would also be etched by the BOE.

4.4 Perforated Support Membrane Structure

Since free-standing electrolyte films proved to be too brittle and prone to failure, supported membranes were examined as a potential solution. The structure is adapted from a design of a palladium film hydrogen purifier proposed in [8]. A silicon nitride/silicon dioxide bilayer is used to provide a stiffened anchor plane for the active film, which is open to gas flows on both sides through circular perforations in the film.

This design also has integrated resistive heaters and temperature sensitive resistors (TSR's) on the membrane, allowing for direct examination of thermal properties of the membrane.

The original holy membrane process is listed in appendix C and diagrammed in figure 4-3. A layer of thermal oxide is first grown on a (100) Si wafer, followed by the deposition of a layer of stoichiometric nitride Si_3N_4. The thermal oxide carries a compressive residual stress, as is to be expected from the insertion of oxygen atoms into the silicon crystal lattice. Stoichiometric nitride, on the other hand, is strongly tensile. The stresses in these films are balanced to minimize later membrane deformation.

The back side of this wafer is patterned in standard positive photoresist with mask in figure D-3. This defines the flow channels formed by the release of the membranes. The nitride is removed with a dry etch in SF_6 and the oxide is removed with a BOE dip, thus forming the KOH hard mask.

The perforations that will eventually allow gas flow to the membrane are then patterned on the front side of the wafer in much the same way with the mask in figure D-5. Only the nitride is etched away this time. The perforations must be aligned with the flow channel mask features to ensure they end up within the released

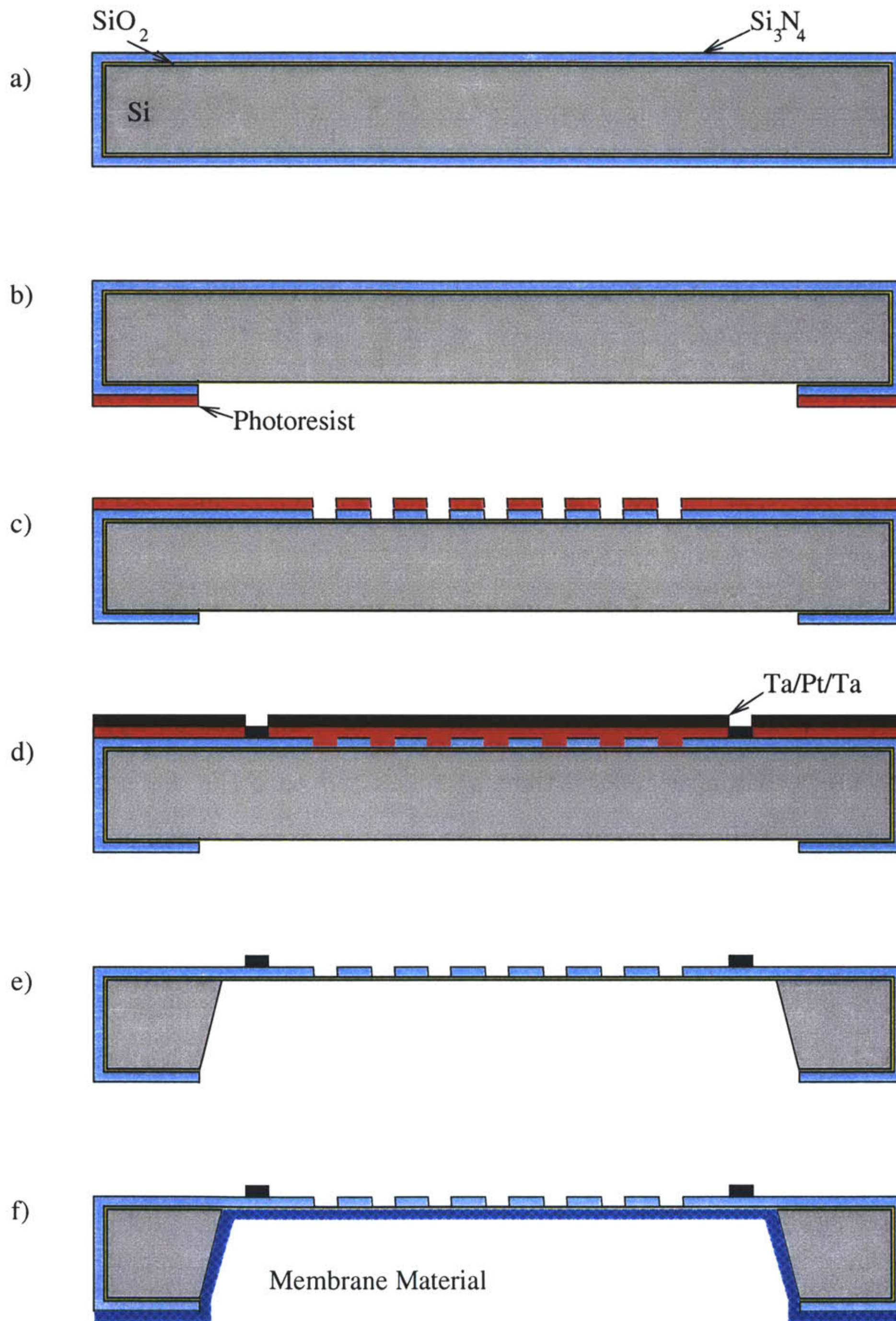

Figure 4-3: Stages in the process to create a perforated nitride supported ("holy") membrane device: (a) Nitride and oxide coated (100) wafer (b) Flow channels hard-masked in nitride and oxide layers by etching through photoresist mask (c) Perforations etched in nitride through photoresist mask (d) Ta/Pt/Ta metalization deposited through image-reverse photoresist pattern (e) Membrane released in KOH (f) Fuel cell materials deposited onto backside of membrane. Once the perforations are opened with BOE, the device is ready to test.

membrane boundary. This is accomplished with complementary registration marks on both masks, using back-side alignment on the EV1 mask aligner/exposer.

Once the hardmasks are patterned, the metalization for the heaters and TSR can then be deposited. The geometry for these is defined with a liftoff process, and is top-side aligned with the registration marks from the perforation mask. The metalization mask in figure D-8 is patterned in image-reverse photoresist. The exposed areas remain upon developing, and so the dark field is cleared of photoresist. The e-beam evaporator is used to coat the front side with a tantalum adhesion layer, the platinum metalization layer, and another tantalum passivation layer. The metals adhere to the wafer only in areas free of resist, and so an acetone dip dissolves away the remaining resist, removing the metal in those regions.

The membranes are then released with the silicon etch. To protect the metalization, a Teflon chuck is used that only permits the wafer backside to contact the KOH solution. KOH has a strong selectivity over SiO_2, and so the etch stops on the oxide layer. The fuel cell materials can then be deposited onto the wafer from the back. The oxide layer is still continuous along the membrane, so a continuous dense film is formed. The perforations are then opened up with a timed BOE dip to remove the oxide and expose both sides of the fuel cell film.

This process was modified slightly later to improve yield and provide more comprehensive data about the fuel cell stack materials. The membranes formed are very fragile, and so minimizing the amount of processing after their release should lessen breakage. Thus, the films are deposited before the KOH etch on the front side instead of the back. The high aspect ratio of the perforation holes, $4\mu m$ in diameter but only 300nm deep, allows the deposition to conformally coat the hole walls and preserve a continuous film.

To prevent the fuel cell materials short circuiting the heaters and TSR's, an insulating layer is used to cover the metalization. The insulation is formed with the mask in figure D-11 in a sequence similar to the metalization, using liftoff on an e-beam evaporated film of aluminum oxide. The final etch in BOE removes the entire oxide layer from the backside flowchannel, and so the SOFC film(s) are supported only on

a perforated nitride membrane.

4.5 Composite Film Test Membrane Structure

It became apparent that the supported film above did not immediately resolve the structural problems with membranes involving the fuel cell materials. In fact, by creating membranes of multiple layers of thin films, stress analysis became increasingly difficult. The earlier free-standing membrane structures were revisited to experimentally characterize behavior in multi-layer film stacks.

Leaving the stoichiometric nitride on the front side of the wafer before depositing the fuel cell stack allows the characterization of nitride and nitride/oxide supported film stacks. The original process without the final timed etch can also be used to explore stacks supported on a VTR nitride layer. These wafers can be measured for residual stress in the film stack after the depositions. Following release, they can be thermally cycled to explore the effects of geometry and film stack composition on mechanical stability.

Chapter 5

Testing Results

5.1 Electrolyte Selection

Prior work characterized free-standing square membranes of electrolyte thin films. Two leading options for the electrolyte material, yttria-stabilized zirconia (YSZ) and gadolinium doped ceria (GDC) were examined, with deposition methods including electron beam (e-beam) evaporation and RF sputtering. These films were heated to investigate membrane robustness.

The test structure had square membranes ranging in side length from $65\mu m$ to $1065\mu m$. All of the membranes formed in this method fractured at temperatures below 700K. Since the minimum temperature for SOFC operation is nearer 800K, free standing electrolyte supported membranes were determined to be inadequate. The collected data is presented in [3]. The tests were useful, however, to narrow the design space as work on supported membranes began.

It was quite evident that the YSZ films were more robust to processing steps as well as thermal treatment than the GDC films. Furthermore, the e-beam evaporated YSZ films tended to have a residual tensile stress, while the sputtered films were compressive, and emerged from deposition buckled. Annealing of the sputtered films for an hour at 600°Cin air relieved the compressive stress and flattened out the film. However, annealing of the e-beam evaporated film, as well as more aggressive annealing of the sputtered film, resulted in the tensile fracture of the membrane, as seen in

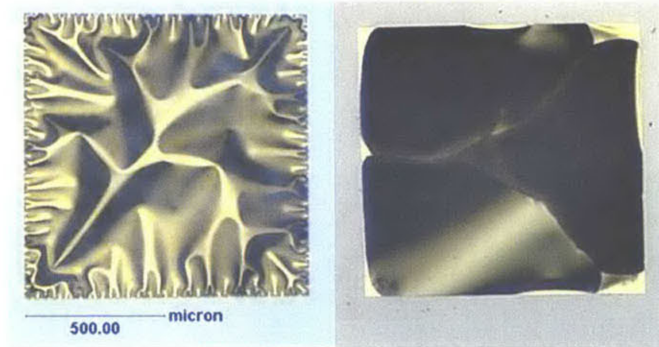

Figure 5-1: As deposited sputtered YSZ membrane buckled due to intrinsic compressive stress on the left; tensile fracture of e-beam evaporated YSZ membrane following anneal on the right.

figure 5-1.

With a CTE of 10×10^{-6} for YSZ compared to silicon's 3×10^{-6} [23], this tensile fracture behavior was certainly unexpected. The membrane would have developed a significant compressive thermal stress upon heating. It was apparent that there were other effects than thermal expansion dictating membrane behavior. It is believed that crystal grain growth is a major contributor.

With the failure of free-standing membranes of sufficient size to survive required temperatures, it was decided that future development work should focus on the design of a supported membrane structure. Based on the results of the heating tests, sputtered YSZ was chosen as the electrolyte layer.

5.2 Supported Membranes

Since large free-standing YSZ membranes were unable to withstand the required temperature range, it was necessary to look into supported membranes. The "holy" membrane proposed in [8] had demonstrated success at supporting non-structural thin palladium films, and so it was decided to adapt that design to support the fuel cell materials.

Several runs were made using the initial perforated membrane process. The support membrane itself was far from mechanically robust; care had to be taken during

processing and handling to minimize breakage of the fragile structures. Problems began at the KOH etch. Some membranes tended to break upon release, and the wafer itself sometimes cracked along fractures initiated at KOH etched corners. The solution was to carefully tighten and loosen the wafer chuck equally around, and monitor the etch closely to avoid drastic overetch.

Dicing the wafer into individual devices also proved disastrous, destroying most of the membranes under conventional conditions. The membranes could be protected with a layer of photoresist, airbrushed over the membranes to avoid contact. Lowering the blade speed and water flow rate on the diesaw also improved membrane survival. These precautions allowed sufficient device yield to enable deposition of the electrolyte material.

The sputtering conditions used were the same as previously used for the free-standing membranes, and so also were expected to produce highly compressive films. Indeed, the first few devices came out of the sputterer with buckled membranes, as seen in figures 5-2 and 5-3. It was decided to anneal these membranes to corroborate the earlier observations of compressive stress relief.

There were two different annealing methods used. A full wafer of released membranes was put in the anneal tube in TRL under a nitrogen flow, and several individual devices were annealed in the Tuller lab in a reducing atmosphere of H_2/N_2. In both cases, all membranes were fractured coming out of the anneal.

A likely candidate for the failure on the full wafer was thermal shock. The anneal tube was initially at 600°C, and so the wafer experienced a rapid temperature increase, blowing out the membranes. The devices annealed in the Tuller lab, however, were ramped at 5°C/min up from and down to room temperature, and still failed. It was hypothesized that the anneal atmosphere was responsible, possibly altering grain formation and growth.

Another run of these devices was attempted. In addition to the low yield, an additional problem was encountered. An airbrushed layer of resist was used to protect the fragile membranes during handling and processing. In the sputterer, however, the wafer got too hot, and hardbaked the resist. It was unable to be removed with acetone,

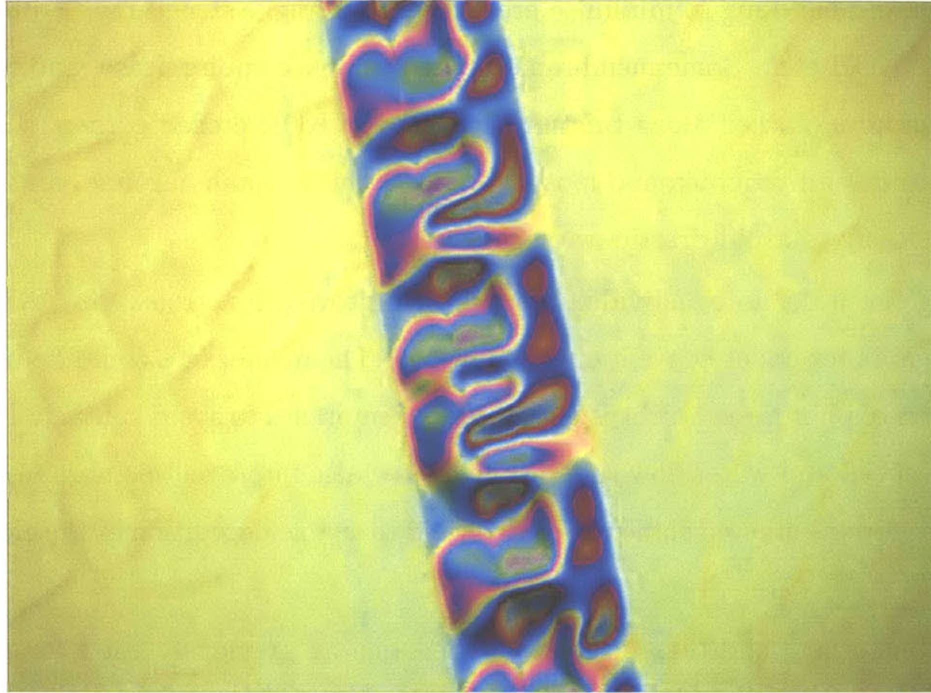

Figure 5-2: A holy membrane is buckled after YSZ deposition. This picture was taken at 5x zoom under polarized light to enhance contrast of the waves.

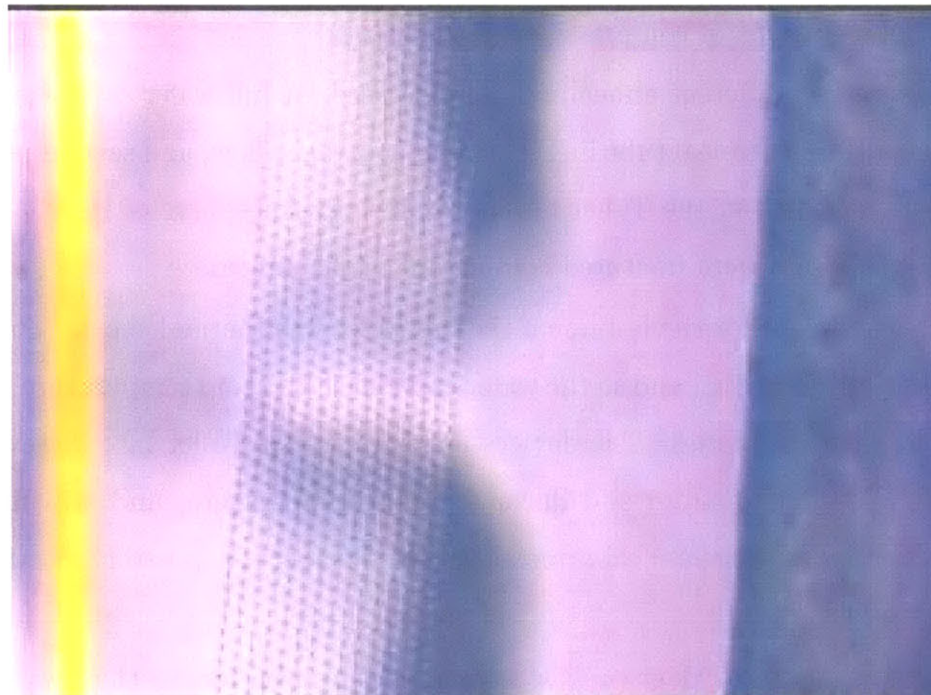

Figure 5-3: A closer look at the buckling on a supported YSZ membrane. The perforations in the nitride layer are clearly visible. This picture was taken under white light at 20x magnification.

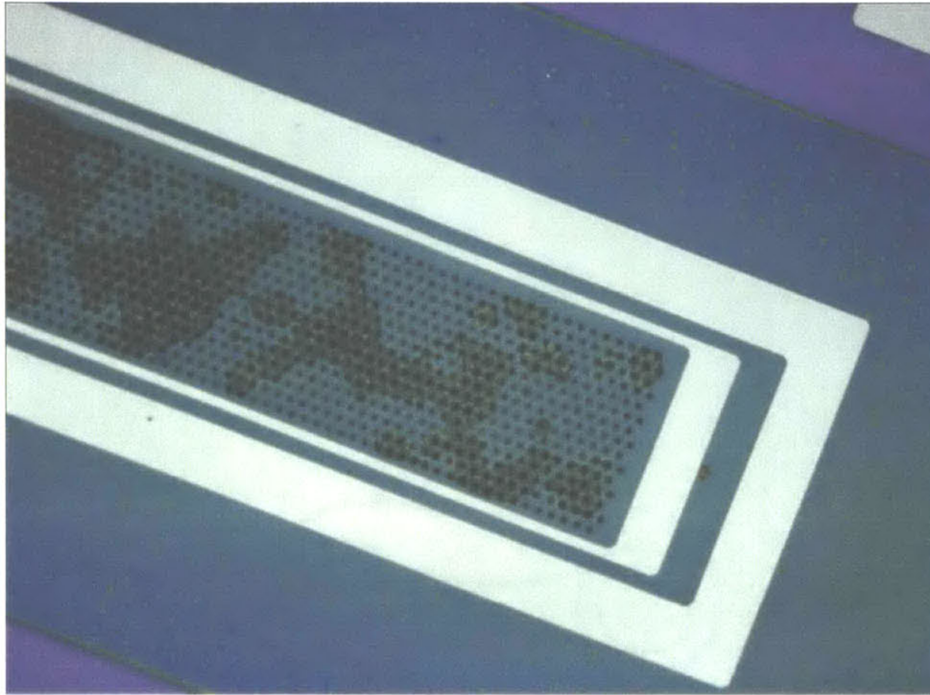

Figure 5-4: A YSZ holy membrane after anneal shows darker regions where the YSZ film has delaminated from the nitride support. This picture was taken at 20x magnification.

as well as a variety of stronger cleaning solutions. A piranha (4:1 H_2SO_4:H_2O_2) clean was the only process able to remove the photoresist, however, it also destroyed the membrane.

A final device did emerge from from the sputterer in a condition for suitable processing. After deposition, the membrane was surprisingly unbuckled. This was annealed to 500°Cfor an hour in air, with a slow ramp rate, and emerged intact. However, micrographs of the device revealed another failure mode. The YSZ film appeared to have delaminated from the nitride support in localized regions, and then buckled where it left the support. This is shown in figures 5-4 and 5-5. This membrane eventually broke due to handling.

As an aside, e-beam evaporation of the YSZ films was briefly revisited to alleviate the bottleneck on the RF sputterer in the Tuller lab. A device was fabricated with a flat membrane following the evaporation. The resistive heaters on this device were then used to raise the temperature at a degree per minute ramp rate, as measured

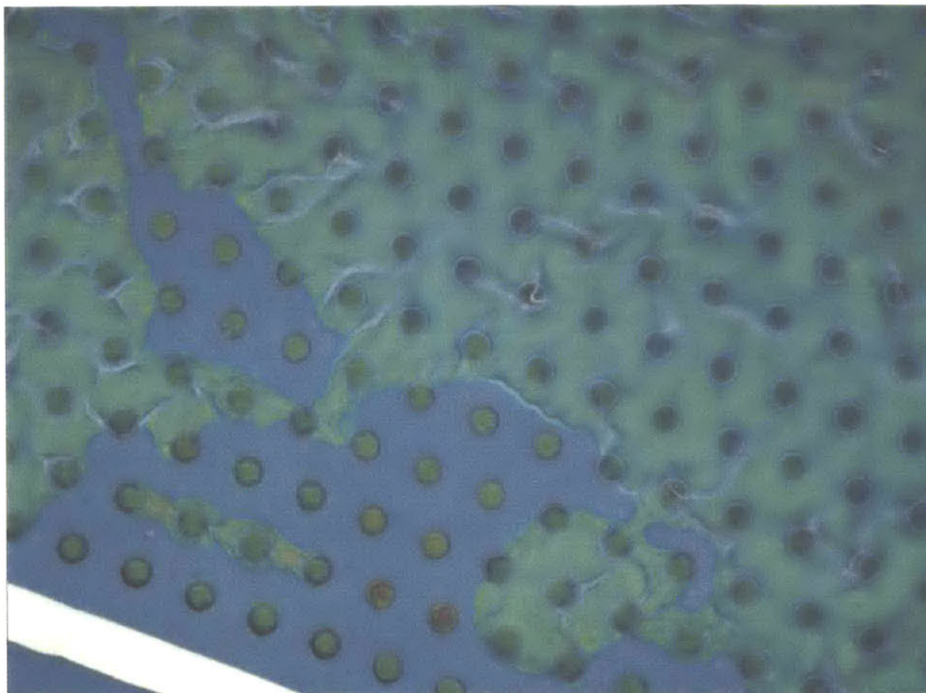

Figure 5-5: A closeup look at 100x on the delaminated regions shows the YSZ film has buckled where it is not bound to the nitride support.

by the TSR. The membrane underwent tensile fracture, as expected from the free-standing film studies, near 258°C. The remains of the membrane are seen attached to the silicon substrate in figure 5-6.

It became apparent that further understanding of YSZ thin-film stresses was needed before membrane devices could be successfully implemented. A final shot-in-the-dark wafer was run with the modified holy membrane process in the hopes that all the pieces might magically fall into place. An entire fuel cell stack was deposited, with co-sputtered platinum-YSZ layers for the electrodes. Platinum, however, has poor adhesion to silicon nitride, and the residual stress in the Pt-YSZ film proved to be too strong. The film cracked and peeled off of the wafer, as seen in figure 5-7, and no useful data was able to be obtained.

Figure 5-6: Pieces of an e-beam deposited YSZ supported membrane remain attached to the substrate following tensile fracture. The membrane was heated with the on-board resistors and failed at 258°C.

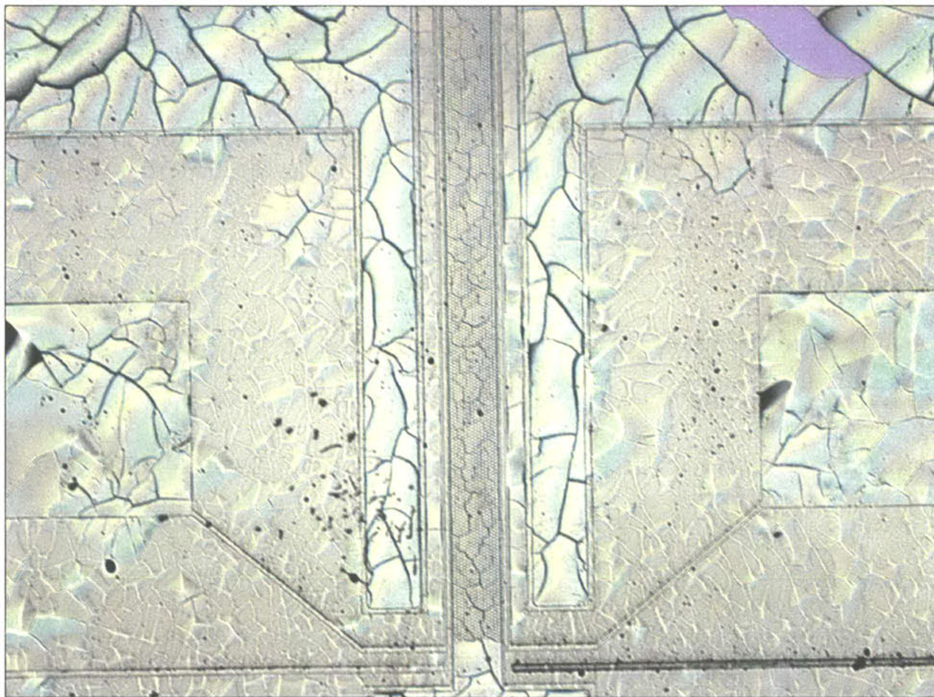

Figure 5-7: The stress in this Pt-YSZ/YSZ/Pt-YSZ film stack was greater than the adhesion to the substrate, and so it delaminated and cracked.

5.3 Stress and Film Characterization

The range of observed membrane behaviors in different runs of what was meant to be the same process indicated that a greater understanding of the underlying effects was required. In particular, film stress dominated membrane behavior, and so it became a priority to predict and control these stresses. Since the added difficulties of multi-layer film stacks also became evident through the previous experiments, both electrolyte and electrode layers needed to be examined.

5.3.1 YSZ Electrolyte Films

The different membrane configurations, namely buckled and flat, observed after sputtered YSZ deposition on holy membrane devices indicated a non-constant film stress. Thus, the effect of processing parameters in the RF sputterer on the resulting film stress was investigated. Films were deposited on one side of a wafer, of which the curvature was measured before and after deposition. The stress of the film could then be calculated from the change in wafer bow.

Many variables could be adjusted; in particular, the applied RF sputtering power, base pressure, atmosphere composition, and substrate temperature were varied. All of these did in fact affect the residual stress in the deposited YSZ films. However, the most significant impact was carried by the base pressure in the sputtering chamber. At low pressures, below 20 mTorr, the deposited films carried a strongly compressive stress. However, above that threshold, the stress became tensile.

At a low base pressure in the chamber, there are few gas molecules to impede the sputtered species on their way to the substrate, and atomic peening effects dominate. As the base pressure increases, the mean free path of incident species decreases due to greater collisions with gas molecules before hitting the surface. Thus, the effects of atomic peening decrease until the grain boundary effects dominate, resulting in tensile residual stress. This range implies an ability to tune the room temperature stress, and so optimize the film in design space as described in section 3.3.4.

5.3.2 Pt-YSZ Electrode Films

Due to the complexity of the specialized electrode materials, deposition techniques and processes are still being examined, so a parametric analysis is still in the future. However, an interim solution is to use a co-sputtered platinum-YSZ cermet film. The platinum serves as a catalyst and current collector, while the YSZ acts as the ionic conductor. Provided each is sufficiently continuous to allow electronic or ionic flow, respectively, the Pt-YSZ film could function as either electrode.

In addition to residual stress, these films also need to be optimized for electric and ionic conductivity. The electrochemical performance is closely tied to the microstructure of the cermet. These are all affected by the aforementioned parameters, including the relative RF power applied to the platinum and YSZ targets, which controls the relative composition. Experiments to characterize these parameters are ongoing.

Chapter 6

Proposed Designs

6.1 Membrane Robustness

The critical point of the fuel cell is the active membrane separating the fuel and oxygen flows. In order to realize a functioning microfabricated solid oxide fuel cell, the problems with the membrane failures must be solved. While work continues on managing the stress in the fuel cell stack thin films, alternate membrane designs are also being considered. There are a variety of alternate fabrication schemes that could potentially improve the mechanical robustness of a membrane.

6.1.1 Honeycomb Supported Membranes

The currently examined design used a perforated nitride film to provide a stiffened support for the brittle SOFC film stack materials. The increase in stiffness required a greater stress to induce buckling, thus proving favorable over a free-standing SOFC stack. However, it did not completely eliminate buckling, and so still ultimately led to failure upon heating at temperatures below those required.

An alternative to the perforated nitride support film is to support the fuel cell stack with a honeycomb structure. This isogrid support would consist of a lattice of tall nitride walls under a perforated nitride film. The fuel cell stack materials could then be deposited on this layer as in the current design. The height of the walls could

be several times the thickness of the nitride film, resulting in a much stiffer structure. Thus, buckling would require much higher stresses, allowing for a greater range in operating temperatures of the device.

Such a membrane could be fabricated by etching narrow trenches in the silicon where the honeycomb walls should be. An isotropic oxide growth followed by nitride deposition would then fill in the trenches to create the walls. Holes in the nitride layer would be patterned between the walls, and the rest of the procedure would be similar to the current test device. The silicon etch would leave just the nitride supported membrane. This process is diagrammed in figure 6-1.

This method has been used in [19] to fabricate a cantilevered beam. The honeycomb membrane sections were demonstrated to be much stiffer than the nitride film membrane alone.

6.1.2 Corrugated Membranes

Another method of stiffening the membrane is to introduce corrugations. As with the isogrid structure, this too can serve to increase the strength of the supporting membrane. A regular pattern of ridges or depressions increases the second moment of the plate, making the structure more resilient to intrinsic stress. Various geometries of corrugated membranes have been shown to suppress bending due to deposited film stress in [10].

Depending on the design, however, corrugations in a membrane can also make it compliant. Linear corrugations tend to stiffen along an axis perpendicular to the ridges, but allow bending along the ridges. This property can be used to surround the active area on a membrane with a compliant boundary. Stresses in the membrane can then be compensated by deformation of this boundary.

This technique has already been used in a variety of devices. In [22], a single corrugation was used to compensate for intrinsic film stress on a deposited thin film membrane. The observed curvature of a free-standing silicon nitride membrane was lower when surrounded by the trench. It also drastically lessened the deflection of the membrane due to thermal stresses. Since a possible failure mode of the fuel

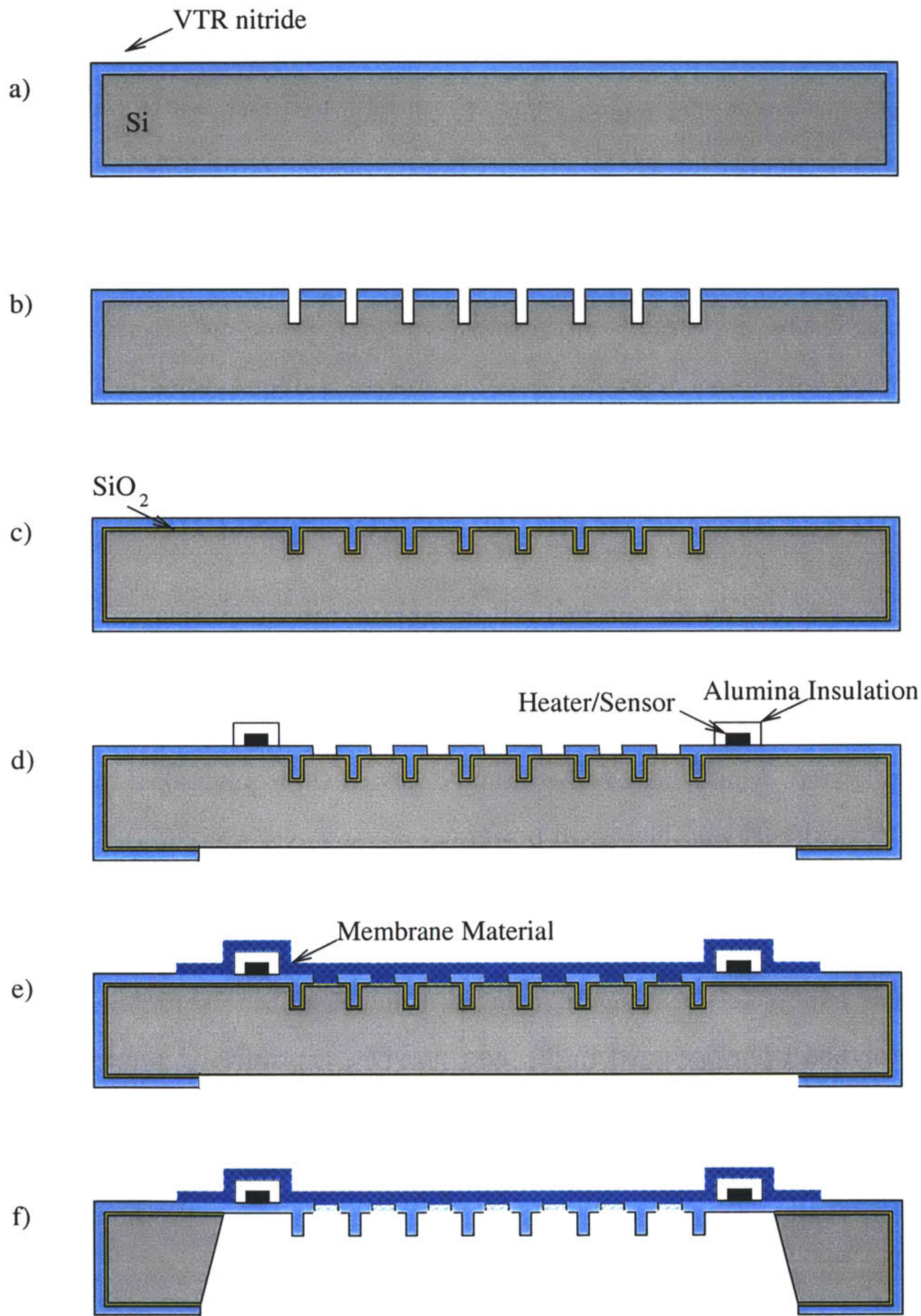

Figure 6-1: Stages in a proposed process to create a honeycomb supported membrane device: (a) Nitride coated (100) wafer (b) Trenches hard masked in nitride etched into silicon (c) Oxide grown and nitride deposited to fill in trenches following stripping of previous nitride mask (d) Perforations hard masked in nitride, flow channels hard masked in nitride and oxide, and metalization and insulation deposited (e) Fuel cell stack deposited on device (f) Membrane released in KOH and perforations opened with BOE.

cell membranes is buckling until fracture, minimizing curvature could significantly improve the robustness of a design.

Corrugations can be formed similarly to the isogrid above, by shaping the silicon substrate before deposition of the support layers. Instead of making narrow trenches, however, wide depressions would be etched in the silicon. After stripping off the etch hardmask, an isotropic silicon etch can be used to round off the corners. Subsequent deposition of oxide and nitride will conform to the depressions. Upon release, then, the membrane will be corrugated [12]. This process is diagrammed in figure 6-2.

6.2 Integrated Portable Power System

Once a successful design for the fuel cell membrane can be fabricated, the next step is to construct a system around it. Incorporating the SOFC component with the associated plumbing and packaging should result in a complete portable power device. Ideally the system would be a self-contained device that only takes in fuel and air, and produces exhaust and electrical power.

The SOFC requires that the membrane be heated to high temperatures during operation. To maximize net electrical power out, it would be beneficial to eliminate the resistive membrane heaters in favor of a chemical heat source. A suspended microreactor has been designed in [2], and provides a promising method of heating the structure through the combustion of fuel. Additionally, this burnbox has strong thermal isolation properties, thus minimizing the power input required to maintain the SOFC at temperature.

A power generation device could be conceived wherein thin-walled silicon nitride tubes deliver fuel and air to an isolated stack of subdevices. Combustion could take place in the burnbox, which would provide heat for the other reactions. A capped fuel cell device similar to the test devices could be bonded to the top of the burnbox, with ports providing the gas flows. This device is illustrated in figure 6-3.

This device is in many ways an ideal prototype system. The two components, namely the combustion box and the fuel cell membrane, are mostly independent.

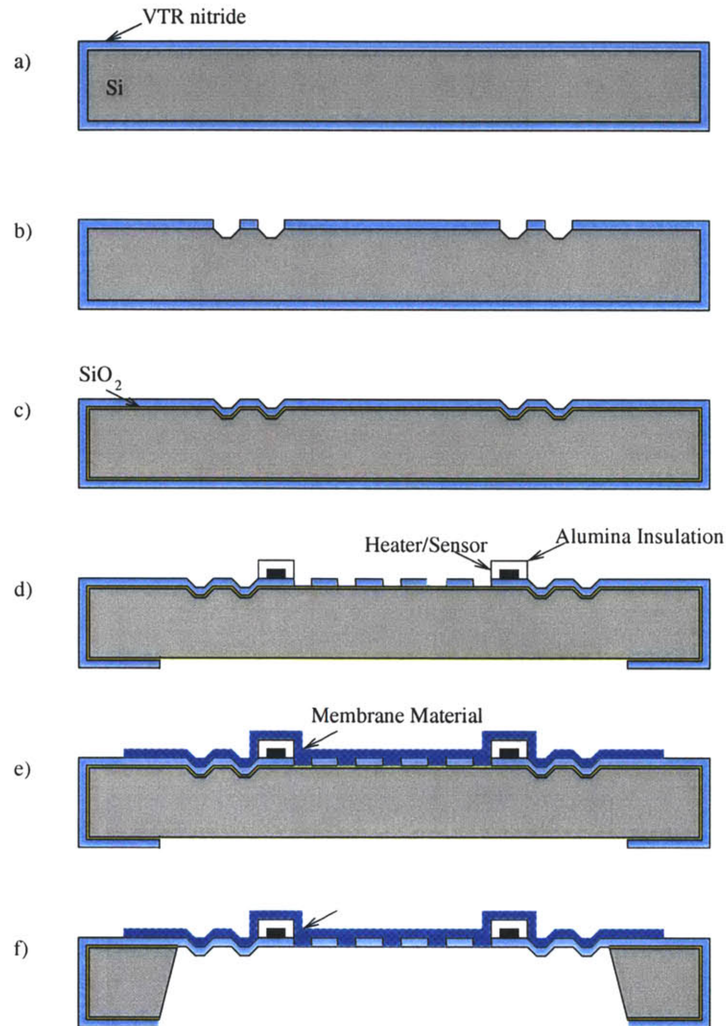

Figure 6-2: Stages in a proposed process to create a corrugated membrane device: (a) Nitride coated (100) wafer (b) Depressions hard masked in nitride etched into silicon (c) Oxide grown and nitride deposited to conform to corrugation pattern following stripping of previous nitride mask (d) Perforations hard masked in nitride, flow channels hard masked in nitride and oxide, and metalization and insulation deposited (e) Fuel cell stack deposited on device (f) Membrane released in KOH and perforations opened with BOE. This schematic illustrates the corrugations being used to make the boundary compliant; they could instead be placed throughout the center region membrane to make it stiffer.

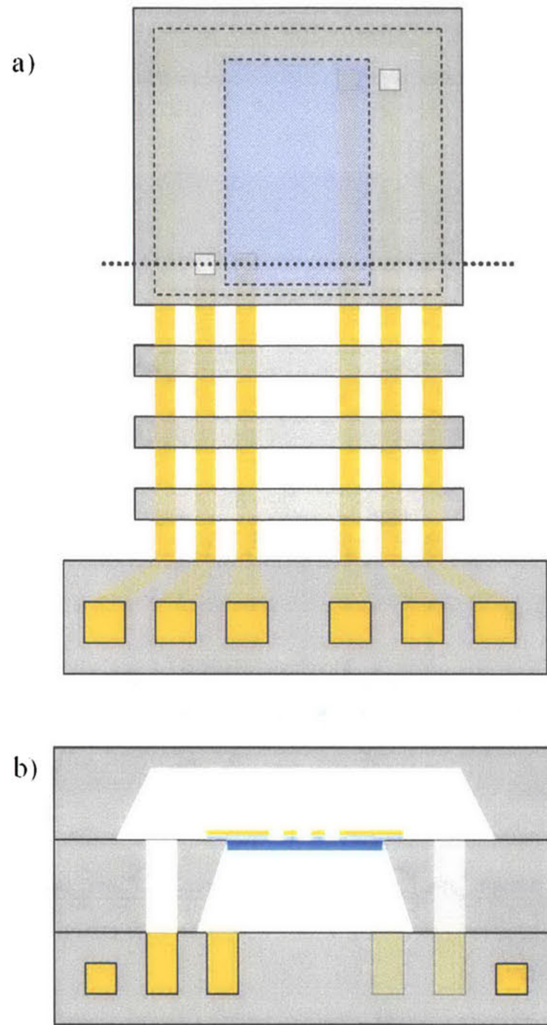

Figure 6-3: A possible design for an integrated SOFC based MEMS power source consists of thin-walled nitride tubes (yellow) feeding gasses to a suspended reaction zone. (a) Top view (b) Cross section through heavy dotted line. Combustion in the outer tube in the bottom block provides heat for operation of the SOFC bonded atop it. The silicon busbars (grey) across the tubes recover heat from exhaust gases, and the device would be vacuum packaged to further minimize energy loss.

They can be fabricated in separate processes, and get bonded right before the final release of the nitride tubes. Thus, most processing issues can be limited to devices that have both received much previous attention.

It also incorporates many of the desired qualities of a SOFC portable power system. The suspended microreactor architecture with a vacuum packaging scheme effectively reduces heat loss to two sources: conduction along the silicon nitride tubes, and convection through the gases exiting the device. Silicon nitride is an excellent thermal insulator, and with the thin walls of the tubes, provides minimal heat loss. The silicon bus bars in the reactor recover much of the heat of the outgoing gases to preheat the incoming gases. Thus, more efficient power conversion can be achieved.

Furthermore, this puts the entire membrane substrate in direct contact with the heat source. Silicon being an excellent heat conductor, the entire stack can largely be considered isothermal. In particular, the silicon anchors for the SOFC membrane will also be at an elevated temperature. This eliminates the thermal stresses in the membrane caused by a non-uniform temperature distribution. With an isothermal membrane and boundary, then, tuning the membrane stress becomes easier, and failure can be more accurately avoided.

This stack can potentially be expanded to include other units, such as a fuel processor/reformer or purifier. The reformer has already been integrated with the burnbox in [2], and the purifier in [8] is of the same form as the fuel cell membrane design. Thus, extending the stack to include these components is a conceivable future design.

Chapter 7

Conclusion

The work presented in this thesis highlights the difficulties inherent in creating a microfabricated solid oxide fuel cell. The operation of a dual-chamber SOFC requires a membrane based structure, and it is this membrane that is the central failure point. The ultimate goal of creating a portable power system is dependant on making this robust enough to survive SOFC operating conditions.

Free standing electrolyte membranes are unstable over the required temperature range, with film stresses invariably resulting in their failure. Thus, a structure must be designed to support the electrolyte. A perforated nitride film support was attempted, but this device is also unable to survive high temperatures.

As with the free standing films, the intrinsic residual stress of the electrolyte typically results in the supported membranes buckling on deposition. Nearly all of these membranes survive deposition intact though, whereas some of the free standing films emerge fractured. However, all fail similarly under annealing or other heating.

These tests result in the observation that there are two fronts that must be pursued in order to achieve a functional fuel cell. The stresses in the films need to be understood and controlled, and a structure needs to be designed that can accomodate large stresses. These investigations have since begun.

YSZ thin films show different stress related behaviors under different deposition and operation conditions. Once this is understood, the correlation between stress and temperature change can be exploited to maximize stability. Also, the additional

complications arising from the multi-layered oxide/nitride/YSZ stack demonstrate the necessity for characterization of all the films including the electrode layers, as well as the stack as a whole.

The currently observed film stresses are such that an additional nitride layer in the membrane is insufficient to prevent failure. Thus, alternate designs are being examined. A honeycomb support with tall thin nitride walls has potential to make the membrane much stiffer and thus resistant to buckling. This stiffening can also be accomplished with corrugations. The physical effects of film stress can be further reduced by surrounding the membrane with a compliant corrugated boundary.

A more robust structure coupled with better stress management in the films should allow for a stable membrane device over the required range of temperatures. This seems a promising path forward, which should result in a microfabricated SOFC. This can then be integrated into a complete portable power system.

Appendix A

Test Membrane Array Process Flow

Table A.1: Revised Test Membrane Array Process

Processing on 4" (100) p-type double-side polished silicon wafer

Color	Step	Description	Equipment	Lab
Black	1	RCA clean wafers	rca1	ICL
Green	2	Oxide growth, 250 nm	5D-FieldOx	ICL
Green	3	Nitride growth, 300 nm	6D-Nitride	ICL
Green	4	apply HMDS	HMDS	ICL
Green	5	apply resist to both sides	coater	TRL
Green	6	pattern backside resist with membrane geometry (mask B-1 or B-2)	EV1	TRL
Green	7	develop resist	photo-wet	TRL
Green	8	post-bake resist	postbake	TRL
Red	9	backside etch nitride layer	plasmaquest	TRL
Red	10	backside etch oxide layer	acid-hood	TRL
Red	(11)	frontside etch nitride layer	plasmaquest	TRL

Continued on next page

Table A.1 – continued from previous page

Color	Step	Description	Equipment	Lab
	12	Deposit fuel cell layers	*	*
	13	Backside KOH etch (with chuck to protect front)	Schmidt Hood	SGL
	(14)	BOE etch wafers to release membranes	acid-hood	EML
	15	die cut wafers into individual devices	diesaw	ICL

Parentheses denote an optional step, based on desired membrane configuration.

* The deposition of the fuel cell stack can either be done on the e-beam evaporator in EML, or the RF sputterer in Harry Tuller's Lab.

Notes

Step 2: Recipe 3W1000 for wet oxidation, runtime 00:25:00 hh:mm:ss. Grow oxide on an additional SSP monitor wafer to use for metrology to measure actual thickness.

Step 3: Recipe 775 DEP for nitride deposition (23 A/min), runtime 02:12:00 hh:mm:ss. Grow nitride on an additional SSP monitor wafer to use for metrology to measure actual thickness.

Step 5: Use standard positive resist, dispense for 5s at 500 RPM, spread for 5s at 750 RPM, spin for 30s at 2000 RPM.

Step 9: Plasmaquest etcher holds wafer with 3 pins, one of which is directly opposite the major flat. Thus n-type wafers are prone to slip off this pin and shatter when the arm comes in. To avoid this, use p-type wafers. Run dummy wafers first to stablize chemistry and calibrate power.

Step 10: BOE dip for approximately 4 minutes, or until features look silver. Dewetting is difficult to observe in such small features.

Step 11: See step 9.

Step 15: To prevent membranes from breaking in the diesaw or with future handling, protect them with photoresist. The airbrush in EML can be used after the KOH etch to coat the frontside with resist without touching the membranes. This can then be rinsed off in acetone prior to use. A lower water flowrate on the diesaw might also be necessary.

Appendix B

Test Membrane Array Masks

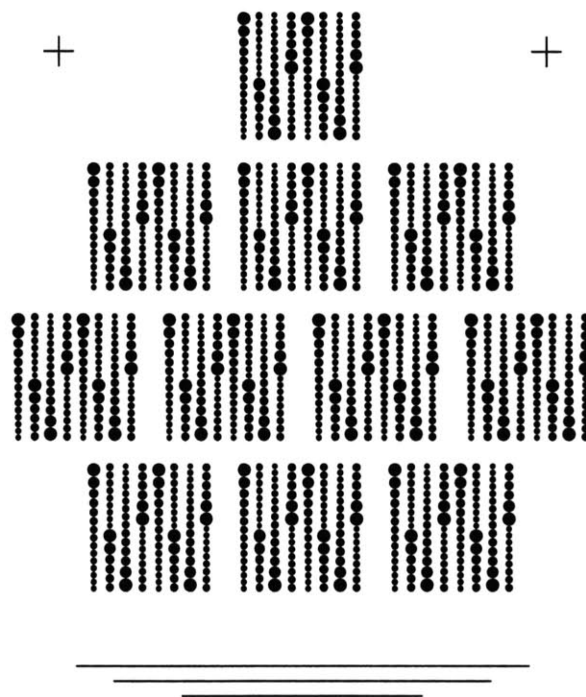

Figure B-1: Nitride etch mask for square variable area test membranes

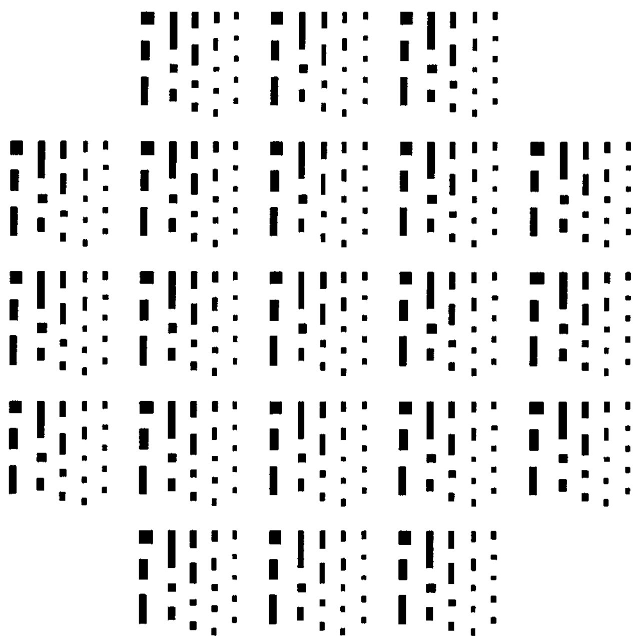

Figure B-2: Nitride etch mask for variable aspect ratio test membranes

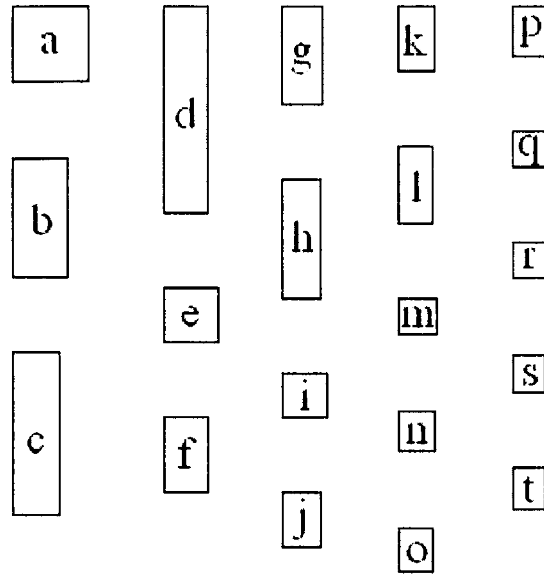

Figure B-3: Die-level nitride etch mask for variable aspect ratio test membranes

Area (μm ^{2})	Aspect ratio			
	1:1	4:1	9:1	16:1
10^6	a, 1000x1000	b, 2000x500	c, 3000x333	d, 4000x250
2.5×10^5	e, 500x500	f, 1000x250	g, 1500x166	h, 2000x125
62500	i, 250x250	j, 500x125	k, 750x83.3	l, 1000x62.5
10000	m, 100x100	n, 200x50	o, 300x33.3	p, 400x25
2500	q, 50x50	r, 100x25	s, 150x16.7	t, 200x12.5

Table B.1: Nominal membrane dimensions for given area and aspect ratio (in μm)

Appendix C

Holy Membrane Process Flow

Table C.1: Holy Membrane Process

Processing on 6" (100) double-side polished silicon wafer

Color	Step	Description	Equipment	Lab
Black	1	RCA clean wafers	rca1	ICL
Green	2	Oxide growth, 250 nm	5D-FieldOx	ICL
Green	3	Nitride growth, 300 nm	6D-Nitride	ICL
Green	4	apply HMDS	HMDS	ICL
Green	5	apply resist to both sides	coater	TRL
Green	6	expose and pattern backside resist to flow channel mask (mask D-3)	EV1	TRL
Green	7	develop resist	photo-wet	TRL
Green	8	post-bake resist	postbake	TRL
Green	9	backside etch nitride layer	LAM490B	ICL
Green	10	backside etch oxide layer using BOE	OxEtch-BOE	ICL
Green	11	piranha remove photoresist	Premetal-Piranha	ICL
Green	12	apply resist to front of wafer	coater6	ICL

Continued on next page

Table C.1 – continued from previous page

Color	Step	Description	Equipment	Lab
Green	13	expose resist to perforations mask (mask D-5)	EV1	TRL
Green	14	develop resist	photo-wet	TRL
Green	15	post-bake resist	postbake	TRL
Green	15	etch nitride layer	LAM490B	ICL
Green	16	piranha remove photoresist	Premetal-Piranha	ICL
Green	17	apply image-reverse photoresist to front	coater	TRL
Green	18	expose resist to circuit mask (for heaters, temp sensor, mask D-8)	EV1	TRL
Green	19	mid-bake resist	prebake	TRL
Green	20	develop resist	photo-wet	TRL
Red	21	apply Ta/Pt/Ta metal layer to top (10:200:20 nm)	eBeamAu	TRL
Red	22	lift-off resist and unwanted Pt/Ta with acetone	photo-wet	TRL
Red	23	Nanostrip wafers to clean acetone residue	acid-hood	TRL
Red	24	apply image-reverse photoresist to front	coater	TRL
Red	25	expose resist to insulation mask (mask D-11)	EV1	TRL
Red	26	mid-bake resist	prebake	TRL
Red	27	develop resist	photo-wet	TRL
Red	28	apply alumina layer over metallization (10 nm)	eBeamAu	TRL
Red	29	lift-off resist and unwanted alumina with acetone	photo-wet	TRL
Red	30	Nanostrip wafers to clean acetone residue	acid-hood	TRL

Continued on next page

Table C.1 – continued from previous page

Color	Step	Description	Equipment	Lab
Red	31	Backside KOH etch (with chuck to protect front)	Schmidt Hood	SGL
Red	32	post-KOH clean, double NH4OH:H2O2:H2O @ 80oC and 50:1 HF Dip (RCA)	acid-hood	TRL
Red	33	anneal metallization @ 650oC for 1 hour under N2	B1-Au	TRL
	34	Deposit fuel cell layers	*	*
	35	BOE etch wafers to open oxide perforations	acid-hood	EML
	36	die cut wafers into individual devices	diesaw	ICL

* The deposition of the fuel cell stack can either be done on the e-beam evaporator in EML, or the RF sputterer in Harry Tuller's Lab.

Notes

Step 2: Recipe 3W1000 for wet oxidation, runtime 00:25:00 hh:mm:ss. Grow oxide on an additional SSP monitor wafer to use for metrology to measure actual thickness.

Step 3: Recipe 775 DEP for nitride deposition (23 A/min), runtime 02:12:00 hh:mm:ss. Grow nitride on an additional SSP monitor wafer to use for metrology to measure actual thickness.

Step 5: Use standard positive resist, dispense for 5s at 500 RPM, spread for 5s at 750 RPM, spin for 30s at 3000 RPM. Frontside coverage is not necessary.

Step 6: Of the 5 rows of devices, two are taped off so that only every other row gets exposed. This decreases the likelyhood of wafer breakage during the KOH etch.

Step 9: Load Nitride cartridge and use 2:30 m:ss primary etch time with 15s overetch.

Step 10: BOE wets oxide, but not silicon, so etch is complete when the BOE solution beads up at the bottom of the flow channels, after about 3 minutes. The channels will appear silver.

Step 11: Asher may be used instead to remove photoresist. Use 4:00 m:ss run time, and verify that all the resist is in fact gone.

Step 12: See step 5.

Step 13: Use the fluoroscope in TRL photoroom after development to ensure resist is cleared from the perforations.

Step 15: Load Nitride cartridge and use 3:00 m:ss primary etch time with 15s overetch.

Step 16: See step 11.

Step 17: Use image-reverse resist, dispense for 12s at 500 RPM, spread for 6s at 750 RPM, spin for 30s at 2000 RPM. To ensure complete coverage, use the longer dispense time to slowly draw the stream out from the center of the wafer, verifying that the bead is wetting the wafer surface. If after spinning there are streaks in the photoresist, wash it off with acetone while spinning the wafer and try again.

Step 20: Watch for the disappearance of interference fringes in the features to indicate the complete removal of photoresist. Use the fluoroscope in TRL photoroom after development to ensure resist is cleared from the features.

Step 21: A thicker platinum layer, up to 400nm, can make liftoff quicker and cleaner.

Step 22: Liftoff usually takes an overnight soak in acetone.

Step 24: See step 17.

Step 27: See step 20.

Step 29: See step 22.

Step 31: Etch in 20% KOH at 80°Cfor approximately 8 hours. Visually inspect the features every 5-10 minutes starting at 7:30 hh:mm to determine the endpoint. The wafer has completely etched through when the membrane regions become clear. After the KOH etch, the wafer is extremely prone to breakage, and so care must be taken in handling. The KOH should not be warmer than 80°Cto allow a gentler etch. The bolts on the waferchuck should be finger-tightened evenly to minimize bending moments in the wafer, and then be loosened before removal.

Step 32: This step is not necessary if the wafer will not go back into TRL, but may still be desired to ensure removal of all KOH residue.

Step 33: Since the fuel cell stack must also be annealed, this step can happen after the next step (fuel cell material deposition) if the anneal conditions can be the same.

Step 34: It was decided to only deposit the materials in the Tuller lab sputterer. The process parameters are variables currently being investigated elsewhere. The sputterer can handle wafers and pieces less than 4" in diameter well, with film uniformity greatest over the center 2" region, falling to very little material near the edges of a 4" piece. A chuck can be used to deposit on a 6" wafer, but this must then sit off of the baseplate. The wafer will then tend to get hotter than in regular operation. A consequence is that any photoresist will hardbake in the chamber and become very difficult (near impossible) to remove. Also since the wafer is sitting off of the baseplate, there will be some deposition on the opposite side. It seems the best option is cutting full wafers into slightly smaller pieces before deposition.

Step 35: The etch can be visually endpointed under a microscope when a halo is visible around the nitride perforations. This is oxide underetch, and care must be taken to avoid complete removal of the oxide layer between the active stack and the nitride support. The approximate time is 3:30 m:ss.

Step 36: To prevent membranes from breaking in the diesaw or with future handling, protect them with photoresist. The airbrush in EML can be used after the KOH etch to coat the frontside with resist without touching the membranes. This can then be rinsed off in acetone prior to use. Also, using UV tape instead of the standard diesaw tape will make later removal much easier and less stressful on the membranes. While cutting, lower the water flow rate to the first tick mark on the gauges.

Appendix D

Holy Membrane Masks

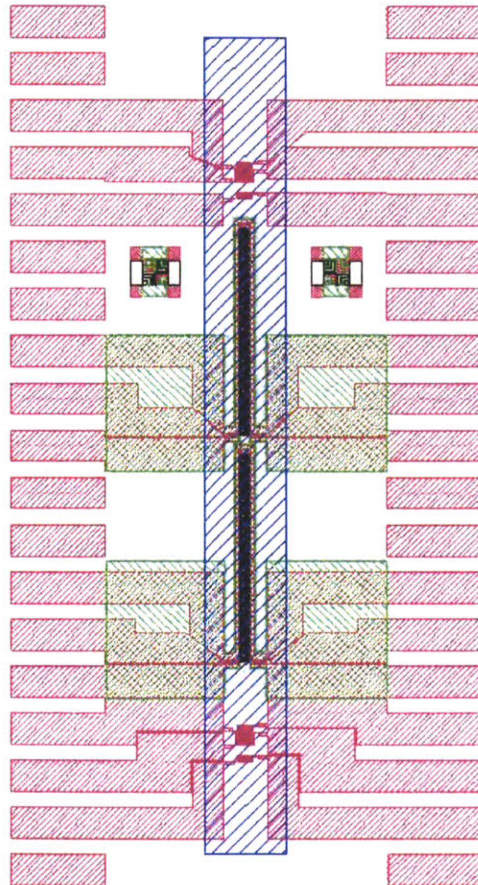

Figure D-1: Die-level masks for holy membrane process: Blue - flowchannel; Black - perforations; Red - metalization; Green - insulation

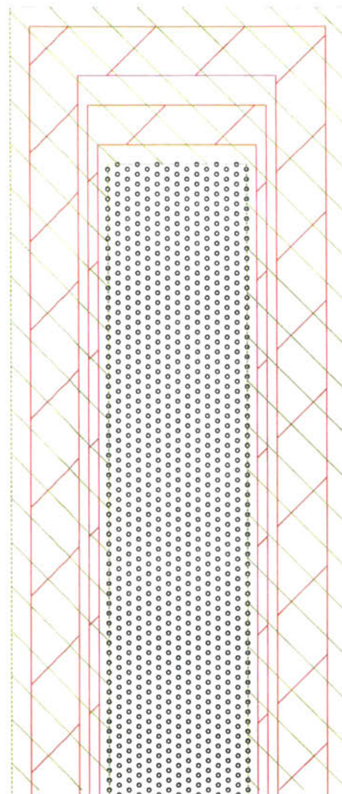

Figure D-2: Top of membrane showing insulation covering metalization around perforations

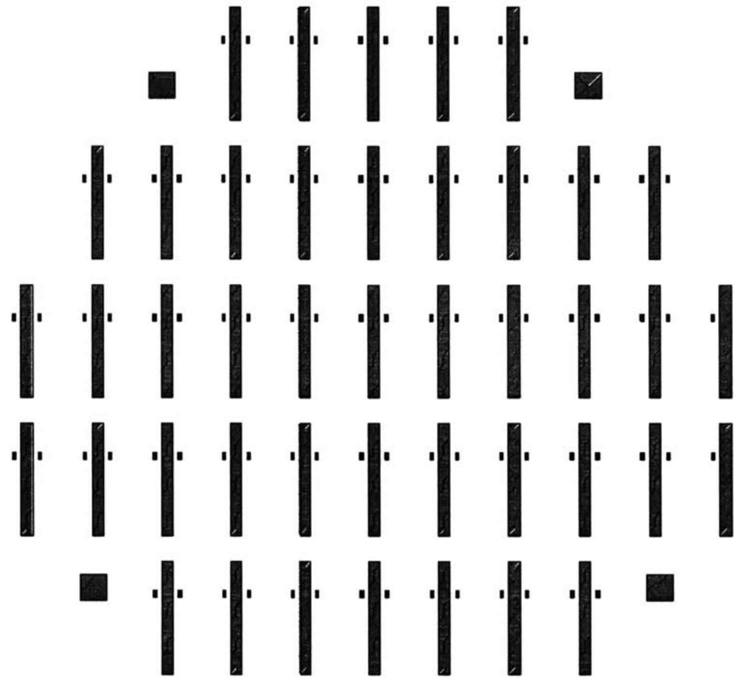

Figure D-3: Flowchannel etch mask in holy membrane process

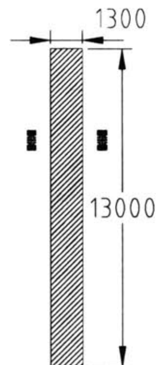

Figure D-4: Die-level flowchannel etch mask, with feature geometry in μm

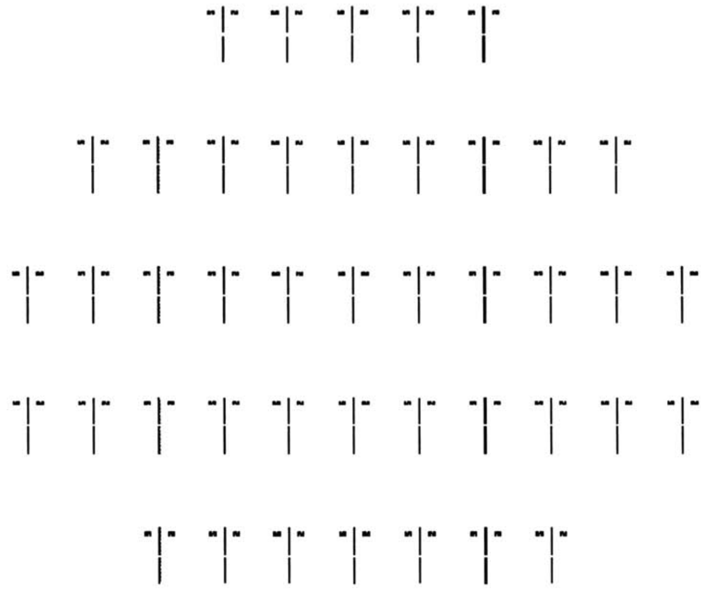

Figure D-5: Perforation etch mask in holy membrane process

Figure D-6: Die-level perforation etch mask

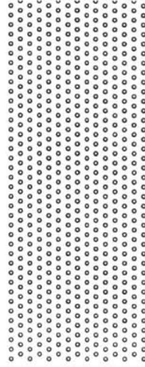

Figure D-7: 4μm perforations in etch mask

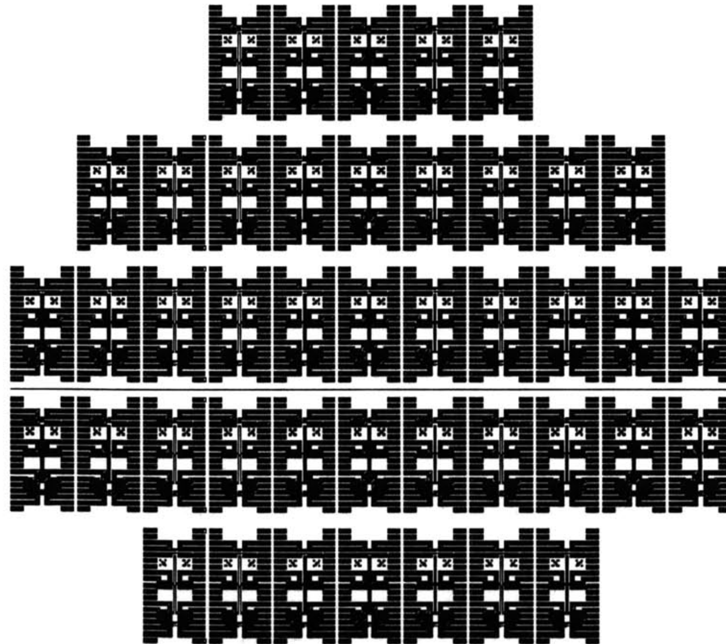

Figure D-8: Metalization liftoff mask in holy membrane process

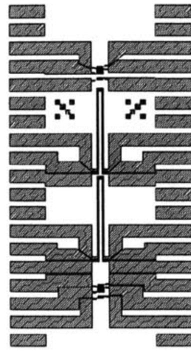

Figure D-9: Die-level metalization liftoff mask

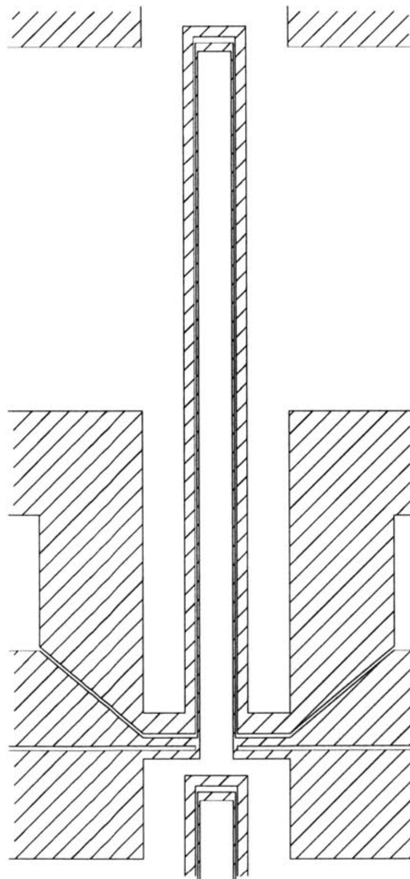

Figure D-10: Temperature sensing wire loop inside heating wire loop on membrane

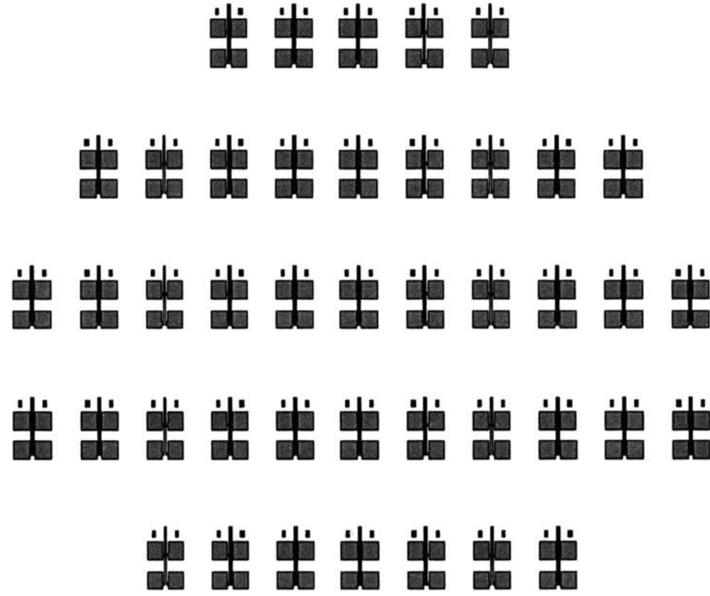

Figure D-11: Insulation liftoff mask in holy membrane process

Figure D-12: Die-level insulation liftoff mask

Bibliography

[1] G. Alberti and M. Casciola. Composite membranes for medium-temperature PEM fuel cells. *Annu. Rev. Mater. Res*, 33:129–54, 2003.

[2] L. Arana. *High-Temperature Microfluidic Systems for Thermally-Efficient Fuel Processing.* PhD thesis, Mass. Inst. of Tech., 2003.

[3] C.D. Baertcsh, K.F. Jensen, J. Hertz, H.L. Tuller, V.T. Srikar, S.M. Spearing, and M.A. Schmidt. Fabrication and structural characterization of self-supporting electrolyte membranes for a micro solid-oxide fuel cell. In preparation for submittal to Journal of Materials Research, 2003.

[4] A. Blum, T. Duvdevani, M. Philosoph, N. Rudoy, and E. Peled. Water-neutral micro direct-methanol fuel cell (DMFC) for portable applications. *J. Power Sources*, 117(1-2):22–25, May 2003.

[5] N.P. Brandon, S. Skinner, and B.C.H. Steele. Recent advances in materials for fuel cells. *Annu. Rev. Mater. Res*, 33:183–213, 2003.

[6] H. Chang, J.R. Kim, J.H. Cho, H.K. Kim, and K.H. Choi. Materials and processes for small fuel cells. *Solid State Ionics*, 148(3-4):601–06, June 2002.

[7] A.H. Epstein et. al. Power MEMS and microengines. In *Proc. Int. Conf. on Solid State Sensors, Actuators and Microsystems (Transducers '97)*, 1997.

[8] A.J. Franz, K.F. Jensen, and M.A. Schmidt. Palladium based micromembranes for hydrogen separation and hydrogenation/dehydrogenation reactions. In *Proc. IEEE MEMS Conference*, pages 382–87, 1999.

[9] J.B. Goodenough. Oxide-ion electrolytes. *Annu. Rev. Mater. Res*, 33:91–128, 2003.

[10] Dan Haronian and Noel C. MacDonald. Spring suspended corrugated membranes. *J. Micromech. Microeng.*, 5:289–96, 1995.

[11] A.F. Jankowski, J.P. Hayes, R.T. Graff, and J.D. Morse. Micro-fabricated thin-film fuel cells for portable power requirements. In *Proc. Mater. Res. Soc. Symp.*, number 730, pages 93–98, 2002.

[12] D. Lapadatu, A. Pyka, J. Dziuban, and R. Puers. Corrugated silicon nitride membranes as suspensions in micromachined silicon accelerometers. *J. Micromech. Microeng.*, 6:73–76, 1996.

[13] M. Morgensen and K. Kammer. Conversion of hydrocarbons in solid oxide fuel cells. *Annu. Rev. Mater. Res*, 33:321–31, 2003.

[14] O.M. Nielsen, L.R. Arana, C.D. Baertsch, K.F. Jensen, and M.A. Schmidt. A thermophotovoltaic micro-generator for portable power applications. In *Proc. Int. Conf. on Solid State Sensors, Actuators and Microsystems (Transducers '03)*, pages 714–17, 2003.

[15] W.D. Nix and B.M. Clemens. Crystallite coalescence: A mechanism for intrinsic tensile stresses in thin films. *J. Mater. Res*, 14:3467–73, August 1999.

[16] S.J. Paddison. Proton conduction mechanisms at low degrees of hydration in sulfonic acid-based polymer electrolyte membranes. *Annu. Rev. Mater. Res*, 33:289–319, 2003.

[17] T. Pichonat, B. Gauthier-Manuel, and D. Hauden. A new proton-conducting porous silicon membrane for small fuel cells.

[18] X. Ren, P. Zelenay, S. Thomas, J. Davey, and S. Gottesfeld. Recent advances in direct methanol fuel cells at los alamos national laboratory. *J. Power Sources*, 86(1-2):111–16, March 2000.

[19] C.A. Savran, A.W. Sparks, J. Sihler, J. Li, W. Wu, D.E. Berlin, T.P. Burg, J. Fritz, M.A. Schmidt, and S.R. Manalis. Fabrication and characterization of a micromechanical sensor for differential detection of nanoscale motions. *J. Microelectromech. Syst.*, 11(6):703–08, December 2002.

[20] S.B. Schaevitz. A MEMS thermoelectric generator. Master's thesis, Mass. Inst. of Tech., 2000.

[21] A.K. Shukla and R.K. Raman. Methanol-resistant oxygen-reduction catalysts for direct methanol fuel cells. *Annu. Rev. Mater. Res*, 33:155–68, 2003.

[22] V.L. Spiering, S. Bouwstra, J.F. Burger, and M. Elwenspoek. Membranes fabricated with a deep single corrugation for package stress reduction and residual stress relief. *J. Micromech. Microeng.*, 3:243–46, 1993.

[23] V.T. Srikar, K.T. Turner, T.Y.A. Ie, and S.M. Spearing. Structural design considerations for micromachined solid-oxide fuel cells. *J. Power Sources*, 125:62–69, 2004.

[24] S. Timoshenko and S. Woinowsky-Krieger. *Theory of Plates and Shells.* McGraw Hill, 2nd edition, 1959.

[25] K. Tuber, M. Zobel, H. Schmidt, and C. Hebling. A polymer electrolyte membrane fuel cell system for powering portable computers. *J. Power Sources*, 122(1):1–8, July 2003.

[26] A.C. Ugural. *Stresses in Plates and Shells.* McGraw Hill, 1999.

[27] Z. Xinge, S. Ohara, K. Mukai, M. Ogawa, and T. Fukui. Effect of chemically etched electrolyte on solid oxide fuel cell performance. *Electrochemistry*, 68(1):11–16, January 2000.

[28] W.C. Young. *Roark's Formulas for Stress and Strain.* McGraw Hill, 1989.